Instability of compressible soft electroactive plates

Article *in* International Journal of Engineering Science · April 2021

DOI: 10.1016/j.ijengsci.2021.103474


Guozhan Xia
Zhejiang University


Yipin Su
Zhejiang University

International Journal of Engineering Science 162 (2021) 103474

Contents lists available at ScienceDirect

International Journal of Engineering Science

journal homepage: www.elsevier.com/locate/ijengsci

Instability of compressible soft electroactive plates

Guozhan Xia[a,b], Yipin Su[a,c,*], Weiqiu Chen[a,b,d,*]

[a] *Key Laboratory of Soft Machines and Smart Devices of Zhejiang Province & Department of Engineering Mechanics, Zhejiang University, Hangzhou, 310027, P.R. China*
[b] *State Key Laboratory of CAD & CG, Zhejiang University, Hangzhou, 310058, P.R. China*
[c] *Sonny Astani Department of Civil and Environmental Engineering, University of Southern California, Los Angeles, CA, 90089, USA*
[d] *Soft Matter Research Center, Zhejiang University, Hangzhou, 310027, P.R. China*

ARTICLE INFO

Article history:
Received 30 January 2021
Revised 12 March 2021
Accepted 16 March 2021

Keywords:
Soft electroactive plate
Surface/wrinkling instability
Dispersion equation
Finite deformation

ABSTRACT

In this paper, we investigate the formation of two-dimensional surface wrinkles in a pre-deformed compressible soft electroactive (SEA) plate. Two common electrical loading protocols are considered: one is the so-called voltage-control where the plate is applied with a constant voltage across the thickness; the other is named as charge-control where the plate is activated by uniformly spraying electrical charges on its main faces. By developing the surface impedance matrix method with the Stroh formulation for compressible SEA materials, we decouple the resulting dispersion equations into symmetric and antisymmetric modes and obtain the associated closed-form expressions, respectively. These analytical expressions of the critical stretch are crucial to the quantitative understanding of wrinkling in the SEA plate. For illustration, we treat examples of compressible Gent and neo-Hookean ideal dielectric elastomers. Results show that the symmetric wrinkles may appear prior to the antisymmetric ones in a sufficiently stretched compressible SEA plate. This phenomenon is in principle caused by the release of incompressibility constraint, upon which the variation of the material chain extension limit only mildly affects the magnitude of the critical stretch. Especially, for charge-controlled plates, a compressibility-driven competition mechanism is revealed that with the increase of compressibility, the symmetric wrinkling is promoted while the antisymmetric one is suppressed. Moreover, enhancing compressibility significantly stabilizes the intrinsic instability of charge-controlled plate while makes the voltage-controlled plate more unstable. These findings, *for the first time*, systematically demonstrate the great significance of material compressibility on the nonlinear response and stability performance of SEA elastomers and can serve a quantitative guidance for the industrial design of new-generation SEA-based devices by exploring the material compressibility.

1. Introduction

Soft electroactive (SEA) materials, e.g., dielectric elastomers (DEs), are smart materials capable of undergoing reversible large deformations when subject to electric stimuli (Pelrine, Kornbluh, Pei, & Joseph, 2000). The coexistence of strong nonlinearity and intrinsic electromechanical coupling makes them ideal candidates for fabricating flexible electronic devices, such as soft robotics, sensors, actuators, and energy harvesters (Acome et al., 2018; Bauer et al., 2014; Lee et al., 2020;

* Corresponding authors.
E-mail addresses: su_yp@zju.edu.cn (Y. Su), chenwq@zju.edu.cn (W. Chen).

https://doi.org/10.1016/j.ijengsci.2021.103474
0020-7225/

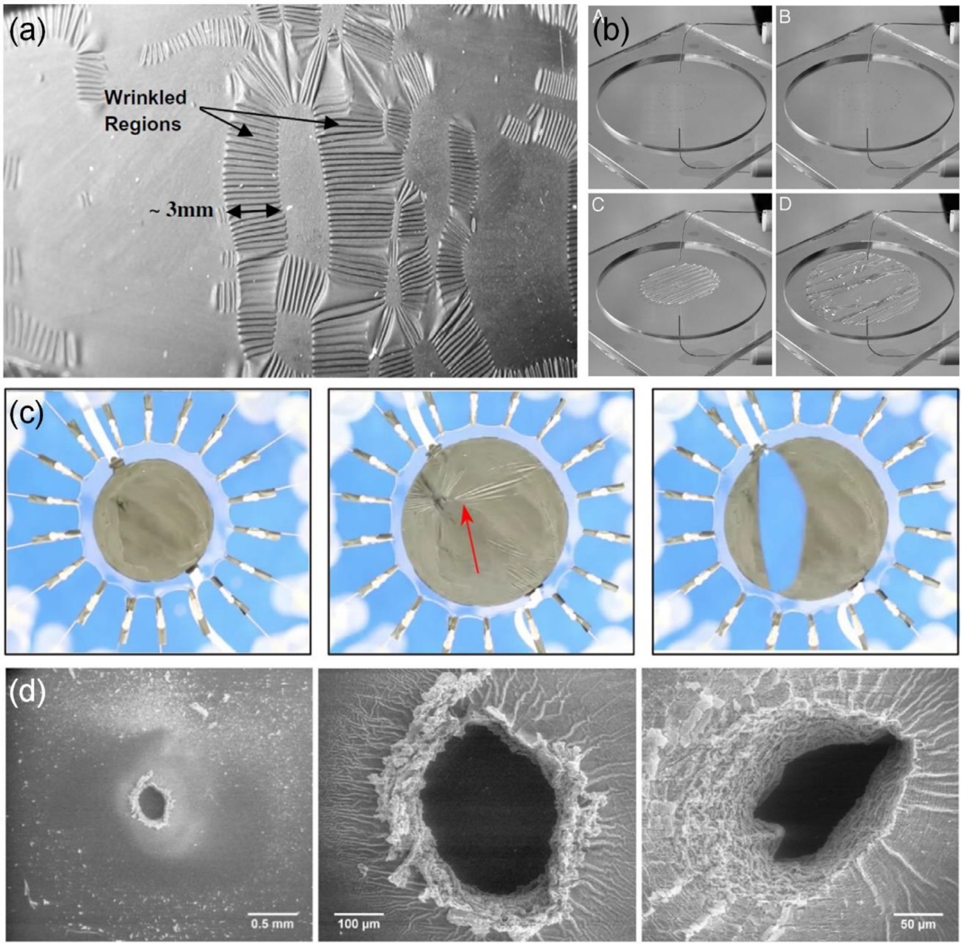

Fig. 1. Experimental observations of various instability patterns of SEA films/plates: (a) the coexistence of two regions, i.e., flat and wrinkled, when applied with a critical voltage (Plante & Dubowsky, 2006); (b) the evolution of wrinkle growth in a fixedly pre-stretched film charged by corona discharge from two needle electrodes (Keplinger et al., 2010); (c) the appearance of wrinkles is almost immediately followed by the pull-in instability in electrically actuated VHB4905 membrane under equi-biaxial dead loads (Greaney et al., 2019); (d) common brittle failures after electrical breakdown (Mateiu et al., 2017).

Mengüç et al., 2014; Mirvakili & Hunter, 2018; Rus & Tolley, 2015). Among rich application circumstances, two electrical loading protocols are commonly employed to generate actuation. One is the so-called *voltage-control* where a constant voltage is applied through compliant electrodes uniformly coated on the top and bottom faces (main faces) of the elastomer (Bortot, Springhetti, & Gei, 2015; Koh et al., 2011; Zurlo, Destrade, & Lu, 2018). Alternatively, *charge-control* generally actives the plate into a deformable capacitor by directly spraying constant electric charges on its main faces (Keplinger, Kaltenbrunner, Arnold, & Bauer, 2010; Li, Zhou, & Chen, 2011; Lu, Keplinger, Arnold, Bauer, & Suo, 2014).

The fantastic performance of SEA devices is however accompanied by the high risk of multiple failure modes, including wrinkling, pull-in, and electrical breakdown (Blok & LeGrand, 1969; Díaz-Calleja, Llovera-Segovia, Dominguez, Rosique, & Lopez, 2013; Mateiu, Yu, & Skov, 2017; Plante & Dubowsky, 2006; Stark & Garton, 1955). When subject to an increasing voltage, an originally flat electroactive film thins down gradually, yielding the further increase of interior true electric field. The film first collapses into complex three-dimensional (3D) wrinkles somewhere and then incurs a dramatic thinning deformation (Plante & Dubowsky, 2006). It is suggested that the wrinkling formation attributes to the out-of-plane buckling induced by relaxation of the in-plane compressive stress (Greaney, Meere, & Zurlo, 2019). And the subsequent thinning phenomenon, also identified as "pull-in" (Stark & Garton, 1955), is due to the positive feedback between the contraction of thickness and the increase of true electric field. It usually results in an irreversible electrical breakdown (Zhao & Suo, 2007). But one should note that the electrical breakdown does not necessarily occur after the pull-in. In fact, the priority essentially depends on the constitutive relation of the specific material (Colonnelli, Saccomandi, & Zurlo, 2015; Su, 2020). All these failures, as depicted in Fig. 1, have long been recognized to pose clear limitations on the development of SEA-based devices.

Many efforts have been devoted to harnessing the pull-in instability and prediction of the electrical breakdown in SEA materials (An, Wang, Cheng, Lu, & Wang, 2015; Bertoldi & Gei, 2011; De Tommasi, Puglisi, Saccomandi, & Zurlo, 2010; Rudykh, Bhattacharya, & deBotton, 2012; Zhao & Suo, 2007; Zhou, Hong, Zhao, Zhang, & Suo, 2008, 2020). Readers may

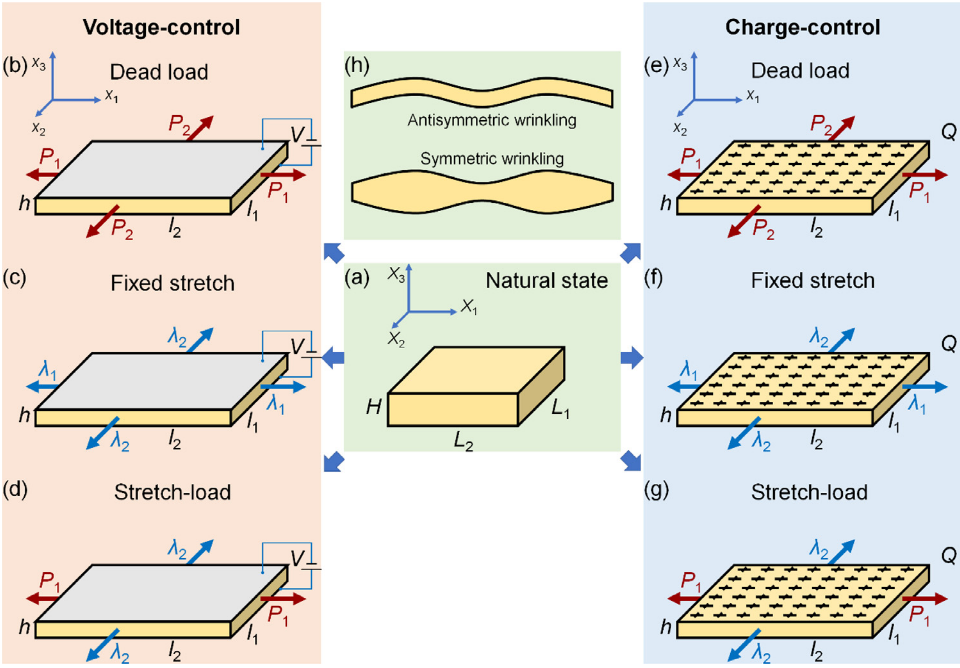

Fig. 2. An SEA plate activated by either a constant voltage (left column) where compliant electrodes (gray) are attached to the top and bottom faces or prescribed charges (right column) where the electrical biasing field is induced by uniformly spraying electric charges on the main faces: (a) an undeformed isotropic compressible SEA plate; (b) and (e) the plate is pre-stressed by in-plane dead loads, i.e. P_1 and P_2; (c) and (f) the plate is constrained to maintain fixed in-plane stretches, i.e. λ_1 and λ_2; (d) and (g) the plate is pre-stressed by the dead load along one in-plane direction ($x_{1(2)}$) and constrained with a fixed stretch in the other direction ($x_{2(1)}$); (h) loss of stability leads to two patterns of wrinkling: antisymmetric and symmetric.

be referred to two recent reviews by Zhu, Zhang, Qian, and Chen (2016) and Lu, Cheng, and Wang (2020) for more details. For example, Zhao and Suo (2007) proposed the so-called Hessian approach to resolve the mechanism of pull- in a voltage-controlled DE plate. They showed that the pull-in instability occurs in the elastomer when the Hessian matrix ceases to be positive definite. This criterion is quite useful for studying the homogeneous instability in SEA materials, yet fails for predicting the inhomogeneous wrinkling instability (Dorfmann & Ogden, 2014; Huang et al., 2012; Su, 2020, 2018a). Unlike the voltage-controlled plate, experimental observations show that no pull-in instability occurs in the SEA actuator operated in a charge-controlled mode, because in this case no positive feedback mechanism increases the true electric field in the elastomer (Keplinger et al., 2010). It is shown that the Hessian matrix of charge-controlled SEA plates has a different form from that of voltage-controlled case and is always positive definite (Conroy Broderick, Righi, Destrade, & Ogden, 2020; Li et al., 2011; Su, Chen, & Destrade, 2019).

In contrast to pull-in and electrical breakdown failures, wrinkles in SEA solids can be controlled and even completely restrained through external electrical loading (Greaney et al., 2019; Keplinger et al., 2010; Liu, Li, Chen, Jia, & Zhou, 2016). This feature has motivated many of the recent theoretical developments in this field. The pioneering work was conducted by Dorfmann and Ogden (2014), investigating the diffuse modes of inhomogeneous wrinkling in incompressible DE plates using the linearized incremental theory. Similar problems were then treated by Díaz-Calleja, Llovera-Segovia, and Quijano-López (2017), Su, Conroy Broderick, Chen, and Destrade (2018b), Yang, Zhao, and Sharma (2017), and Conroy Broderick et al. (2020) from different theoretical aspects. It is of interest that the last two works employed the so-called surface impedance matrix method and the Stroh formulation (Destrade, 2015) so that all the results were obtained in a fully analytical manner. The theoretical analysis for incompressible voltage-controlled plates agrees well with the experimental observation (Plante & Dubowsky, 2006; Su et al., 2018b), while it looks not that apparent for the charge-controlled ones (Conroy Broderick et al., 2020; Keplinger et al., 2010). This conflict is actually due to the application of different mechanical loading protocols: (i) no wrinkle occurs when the plate is loaded by biaxial dead loads, because the monotonic loading curves never enter the unstable region (Conroy Broderick et al., 2020); (ii) When constrained by fixed in-plane stretches, e.g., radially pre-stretched first and then fixed on a rigid frame (Keplinger et al., 2010), the plate naturally wrinkles once the electric stimulus reaches a certain threshold value, which is actually consistent with the theoretical prediction (Conroy Broderick et al., 2020).

Although the electric-induced instability of incompressible SEA materials has been fairly well described, the effect of compressibility is usually ignored and less understood. To our best knowledge, the only work concerning this aspect was devoted by Liu, Liu, Leng, and Lau (2011), suggesting that the Poisson's ratio be positively correlated to the critical nominal electric field for the onset of pull- in tri-axially stretched Varga type DEs. On the contrary, when electric stimuli are absent, it has been extensively shown that the variation of compressibility significantly impacts the physical behaviors of soft materials, such as nonlinear response (Levinson & Burgess, 1971; Ogden, 1972; Rogovoy, 2001), wave propagation (Destrade & Saccomandi, 2005; Dowaikh & Ogden, 1991; Ogden & Sotiropoulos, 1998), Euler buckling (Burgess & Levinson, 1972; Murphy & Destrade, 2009). In addition, fabrication of compressible SEA-based devices is recently emerging as an exciting and promising field in research communities (Carrara et al., 2020; Cheng et al., 2020; Lee et al., 2020; Loeb, Amert, & Whites, 2014; Wan et al., 2018; Yang et al., 2020). Thus, a comprehensive study on the role of compressibility in electric-induced instability is of considerable theoretical and practical significances, especially for understanding the failure mechanism and the performance optimization of such SEA-based devices.

Encouraged by the significant compressibility of emerging SEA materials and the lack of theoretical research on the corresponding problems, this paper mainly pursues a general analysis for the surface/wrinkling instability of a pre-deformed compressible SEA plate. This plate is subject to in-plane mechanical and transverse electrical biasing fields, which is performed through one of several common loading protocols as shown in Fig. 2. Upon the finitely deformed configuration, an arbitrary but infinitesimal perturbation is superimposed. The onset of wrinkling can be seen by that equilibrium equations for the perturbation exist more than one non-trivial solution. It is noted that with a given electrical actuation, either voltage-control or charge-control, and no dissipative effect, the wrinkling instability of an SEA plate should essentially depend only on the deformation state rather than the mechanical loading paths or methods.

This paper, *for the first time*, systematically investigates the role of material compressibility on the nonlinear response and instability of SEA materials, thus can provide solid reference for design and fabrication of SEA-based devices using a much wider range of material candidates. The paper is structured as follows.

In Section 2, we investigate the instability behaviors of a compressible voltage-controlled SEA plate under biasing fields. First, the nonlinear response of the plate under finite deformation is proposed when subject to in-plane equi-biaxial stretches and a transverse voltage. Then, we establish analytical dispersion relations for the symmetric and antisymmetric wrinkling instabilities, respectively. The explicit expressions for the thin-plate (long-wave) and thick-plate (short-wave) limits are also provided, with which we can define the global and wavelength-independent instability domains for plates with specific dimensions.

In Section 3, we present parallel results for a compressible charge-controlled plate in a similar fashion in Section 2. Unlike the voltage-controlled scenario where the nominal electric field is concerned, all the results in this case are correlated to the nominal electric displacement.

In the above two sections we only present simplified expressions for SEA plates of specified energy functions, full details of the derivation for a general energy function are given in Appendices A and B, including the theory of nonlinear electroelasticity (Dorfmann & Ogden, 2010b; Toupin, 1956), the linearized incremental theory (Bertoldi & Gei, 2011; Bortot & Shmuel, 2018; Dorfmann & Ogden, 2010a; Rudykh & deBotton, 2011; Su et al., 2019; Xia, Huang, Su, & Chen, 2020), and the surface impedance matrix method first proposed for compressible SEA materials.

For illustration, we specialize in equi-biaxially stretched plates and numerical calculations are given in case of Gent ideal dielectric, which accounts the strain stiffening effect of most polymers, and also in case of neo-Hookean ideal dielectric, referred to as a special Gent material with infinite extensibility. It should be highlighted that, in contrast to the incompressible case, the symmetric wrinkling in compressible plates may appear prior to the antisymmetric one regardless of the electrical loading protocols.

In Section 4, we further compare the surface instability between voltage- and charge-controlled cases using thin-plate and short-wave limits. All the critical curves are plotted in terms of true electric displacement in an intrinsic way. Most interestingly, the increase of compressibility shows a stabilization effect for the charge-controlled plate while makes the voltage-controlled plate more susceptible to wrinkling. While the intrinsic instability is independent of the electrical loading protocols in the incompressible case, a compressible SEA plate is always more stable under the charge-controlled actuation if the effective true electric loading keeps unchanged.

Finally, we draw conclusions and outlooks in Section 5.

2. Voltage-controlled compressible SEA plate

In this section, we consider the instability of a compressible voltage-controlled SEA plate originally in the natural state, see, Fig. 2(a), with an initial size of $L_1 \times L_2 \times H$ (length $\times$ width $\times$ thickness). With a constant voltage, V, applied across its thickness, the plate deforms into a new configuration of $l_1 \times l_2 \times h$ through different mechanical loading protocols as shown in Figs. 2 (b-d). Such a homogeneous deformation can be described by the principal stretches in three dimensions, i.e., $\lambda_1 = l_1/L_1$, $\lambda_2 = l_2/L_2$ and $\chi = h/H$, respectively. For convenience, we here replace the voltage equivalently by a transverse nominal electric field: $E_0 = V/H$.

For the wrinkling formation, the technical procedures of generalized instability analysis are conducted in the appendices for a general free energy density function, Ω. In the main text, we specialize the discussion to the compressible Gent ideal dielectric, governed by $\Omega_{\rm G} = W_{\rm G}(I_1, I_3) + I_5/(2\varepsilon I_3^{1/2})$, and the compressible neo-Hookean ideal dielectric, described by $\Omega_{\rm nH} = W_{\rm nH}(I_1, I_3) + I_5/(2\varepsilon I_3^{1/2})$. The definitions of $W_{\rm G}$, $W_{\rm nH}$, I_1, I_3, I_5, and ε can be found in Appendix A. Here the material compressibility is considered by assuming the energy density function is dependent on $I_3 = J^2$, with J being the local volume change ratio. Note that the corresponding energy density function for the incompressible elastomer can be obtained by taking $I_3 = 1$ (Gent, 1996; Holzapfel, 2000; Horgan & Saccomandi, 2004; Xia et al., 2020). In particular, we treat the example of equi-biaxial deformation (i.e., $\lambda_1 = \lambda_2 = \lambda$) for illustration. One may note that the mixed-boundary problem as shown in Fig. 2(d) is in general not equi-biaxial, yet its instability behaviors can be resolved in a similar way without any difficulty.

2.1. Nonlinear response

The nonlinear response of SEA materials can be well captured by the theory of nonlinear electroelasticity (Dorfmann & Ogden, 2010b; Toupin, 1956). For the considered problem, we regard E_0 as the prescribed variable, i.e., E_{l3} defined in Appendix A.1. The only nonzero component of the true electric displacement in the thickness direction then adjusts according to the formula $D_3 = \varepsilon E_0/\chi$.

In view of Eq. (A13), for an equi-biaxially deformed SEA plate subject to nominal in-plane stress, we have the following non-dimensional nonlinear response for the Gent ideal dielectric type

$$\bar{s} = \frac{\lambda\left(1-\chi^2/\lambda^2\right)}{1-(I_1-3)/J_\mathrm{m}} - \bar{E}_0^2\lambda/\chi, \tag{1}$$

where J_m is the chain extension limit, also called dimensionless stiffening parameter,$\bar{s} = s/\mu$ and $\bar{E}_0$=E$_0/\sqrt{\mu/\varepsilon}$ are the non-dimensional measures of the nominal in-plane stress and nominal electric field, with μ and ε being the initial shear modulus and the permittivity of the material, respectively.

The corresponding neo-Hookean version can also be easily obtained as $J_\mathrm{m} \to \infty$ in Eq. (1):

$$\bar{s} = \lambda\left(1-\chi^2/\lambda^2\right) - \bar{E}_0^2\lambda/\chi. \tag{2}$$

Hereinafter, the overbar is always used to indicate the nondimensional quantities unless otherwise stated.

2.2. Inhomogeneous and small-amplitude wrinkling

We now focus on the formation of small-amplitude two-dimensional (2D) wrinkles appearing on the mechanically-free faces of the plate. Without loss of generality, the wrinkles are assumed harmonic in the x_1-direction, and the induced incremental fields has a plane-strain character only existing in the $x_1 - x_3$ plane. The solving routine is briefly described as follows (readers may be referred to Appendix B for complete details):

(1) Rely on the linearized incremental theory to derive the governing equations;
(2) Formulate the boundary value problem in the Stroh form;
(3) Solve the incremental boundary value problem using the surface impedance matrix method to obtain the dispersion relations.

In our analysis, the traction-free condition always holds in the free-standing plate, while the incremental electrical boundary condition is implied by the given electrical actuation. That is, the incremental electric potential automatically vanishes on the main faces of the voltage-controlled plate. To be highlighted, the equations of Stroh form derived for the compressible SEA materials perfectly recover the incompressible case when the incompressible limit is applied, as in the purely elastic problem (Destrade, Martin, & Ting, 2002).

As an illustration, we present analytical expressions for the neo-Hookean ideal dielectric plate. Working with Eqs. (B24), (B26) and (B40), we have a simple dispersion relation for the wrinkling:

$$\frac{\left(r_2^2+1\right)^2}{(r_2^2-1)r_2r_3}\left[\frac{\tanh(r_3\chi\pi H/\mathcal{L})}{\tanh(\chi\pi H/\mathcal{L})}\right]^{\pm1} - \frac{4}{r_2^2-1}\left[\frac{\tanh(r_2\chi\pi H/\mathcal{L})}{\tanh(\chi\pi H/\mathcal{L})}\right]^{\pm1} = \lambda\bar{D}_3^2, \tag{3}$$

where $r_2 = \lambda/\chi$, and $r_3 = \sqrt{1-(\chi^{-1}-\lambda^{-2}\chi)/[2(\overline{D}_3^2 - 2J^3\overline{\Omega}_{33})]}$ with $J = \lambda^2\chi$, $\overline{\Omega}_{33} = \partial^2(\Omega_\mathrm{nH}/\mu)/\partial I_3^2$ and $\mathcal{L}$ is the "wavelength" of wrinkles. Here and below, the $+1$ (-1) exponent corresponds to the anti-symmetric (symmetric) wrinkling.

Then we substitute the relationship $\bar{D}_3 = \bar{E}_0/\chi$ into Eq. (3) to get the version in terms of the nominal electric field

$$\frac{\left(r_2^2+1\right)^2}{(r_2^2-1)r_2r_3}\left[\frac{\tanh(r_3\chi\pi H/\mathcal{L})}{\tanh(r_1\chi\pi H/\mathcal{L})}\right]^{\pm1} - \frac{4}{r_2^2-1}\left[\frac{\tanh(r_2\chi\pi H/\mathcal{L})}{\tanh(r_1\chi\pi H/\mathcal{L})}\right]^{\pm1} = \lambda\chi^{-2}\bar{E}_0^2, \tag{4}$$

where $r_3 = \sqrt{1-(\chi^{-1}-\lambda^{-2}\chi)/[2(\chi^{-2}\overline{E}_0^2 - 2J^3\overline{\Omega}_{33})]}$ accordingly.

By replacing the terms of "tanh (*)" with 1 in Eq. (4), we get the so-called short-wave limit (SWL) of dispersion equation as

$$\frac{\left(r_2^2+1\right)^2}{(r_2^2-1)r_2r_3} - \frac{4}{r_2^2-1} = \lambda\chi^{-2}\bar{E}_0^2. \tag{5}$$

Note that the results of Su et al. (2018b) can also be reproduced from Eq. (4) as $\nu \to 0.5$, i.e.,

$$\frac{\left(1+\lambda^6\right)^2}{4\lambda^3} + \frac{\lambda^5(1-\lambda^6)}{4}\bar{E}_0^2 = \left[\frac{\tanh\left(\lambda\pi H/\mathcal{L}\right)}{\tanh\left(\lambda^{-2}\pi H/\mathcal{L}\right)}\right]^{\pm1}, \tag{6}$$

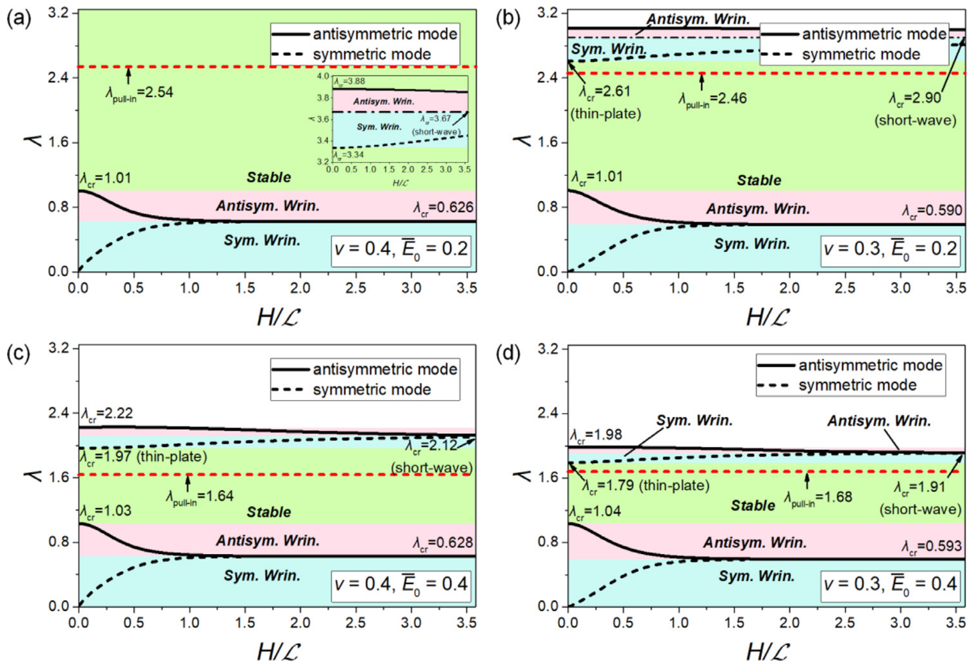

Fig. 3. Phase diagrams of wrinkling instability for equi-biaxially stretched voltage-controlled neo-Hookean ideal SEA plates, where the black solid and dashed lines are the dispersion curves for the antisymmetric and symmetric wrinkles, respectively, and the red horizontal dashed lines correspond to the onset of pull-in instability: (a) $\nu = 0.4$ and $\bar{E}_0 = 0.2$; (b) $\nu = 0.3$ and $\bar{E}_0 = 0.2$; (c) $\nu = 0.4$ and $\bar{E}_0 = 0.4$; (d) $\nu = 0.3$ and $\bar{E}_0 = 0.4$. The lower dispersion curves correspond to the wrinkling in contraction, and the upper ones, if exist, are for that in extension. The stable and wrinkled regions are clearly clarified by colors and/or notes. Hereinafter, "*Antisym. Wrin.*", "*Sym. Wrin.*" are the abbreviations of "antisymmetric wrinkling" and "symmetric wrinkling", respectively.

and the purely elastic criterion of buckling can be reduced by taking $\bar{E}_0 = 0$ (Ogden & Roxburgh, 1993).

For the extremely thin plate, instead of the substitution of $H/\mathcal{L} \to 0$ into Eq. (4), we employ a more general way as done in the incompressible case (Su et al., 2018b) to give the expressions in Eqs. (B30) and (B33) for the so-called thin-plate limit (TPL) of symmetric and antisymmetric modes, respectively.

2.2.1. Example: neo-Hookean ideal SEA plate

We plot the phase diagrams of wrinkling instability for the neo-Hookean ideal SEA plates of different compressibility applied with sequential bias voltages in Fig. 3, of which three sets of complete cases are shown in Figs. C1–C3.

As seen in Figs. 3 (a, b), for $\bar{E}_0 = 0.2$ (low voltage) and (c, d) for $\bar{E}_0 = 0.4$ (high voltage), both the slightly compressible ($\nu = 0.4$) and moderately compressible ($\nu = 0.3$) plates can wrinkle in contraction or in extension. The general existence of such two modes of wrinkling can be verified by the fact in Figs. C4 (a, b) that the thin-plate and short-wave dispersion curves have two critical values at a fixed voltage, where the smaller one corresponds to the contractile wrinkling and the larger one is for the extensional wrinkling.

Moreover, the stable region of the moderately compressible plate has a lower upper bound but a bit higher lower bound than that of the slightly compressible one. It suggests that the plate with higher compressibility is more apt to wrinkle. This is quite reasonable, because the constraint of incompressibility may to some extent provide a stabilizing effect when confining the deformation. More interestingly, unlike the incompressible case, the symmetric wrinkles here may appear prior to the antisymmetric ones in extension, while the antisymmetric mode keeps dominant in contraction.

With the pull-in instability further considered, as highlighted by red dashed horizontal lines in Fig. 3, we can see that the critical stretch for the pull-in, $\lambda_{\mathrm{pull}-in}$, is smaller than that for the wrinkling in extension. However, it should be mentioned that the priority of instability can be significantly tuned by the loading protocol (Su et al., 2019). One typical example is that pull-in never emerges in a voltage-controlled SEA plate constrained by fixed stretches. Besides, for the cases that pull-in indeed occurs, the plate with a smaller Poisson's ratio possesses a smaller $\lambda_{\mathrm{pull}-in}$ at the low voltage ($\bar{E}_0 = 0.2$) while the result reverses when subject to the high voltage ($\bar{E}_0 = 0.4$). A global view of such a non-monotonic phenomenon can be found in Figs. C4 (c, d).

2.2.2. Example: Gent ideal dielectric plate

It should be noted that actual SEA materials may suffer irreversible strain-induced crystallization when overly stretched (Nah et al., 2010), which is usually explained by the strain stiffening effect. Hence, it may be also necessary to examine the effect of chain extension limit on wrinkling behaviors. In Fig. 4, we plot dispersion curves for the wrinkling in incompressible

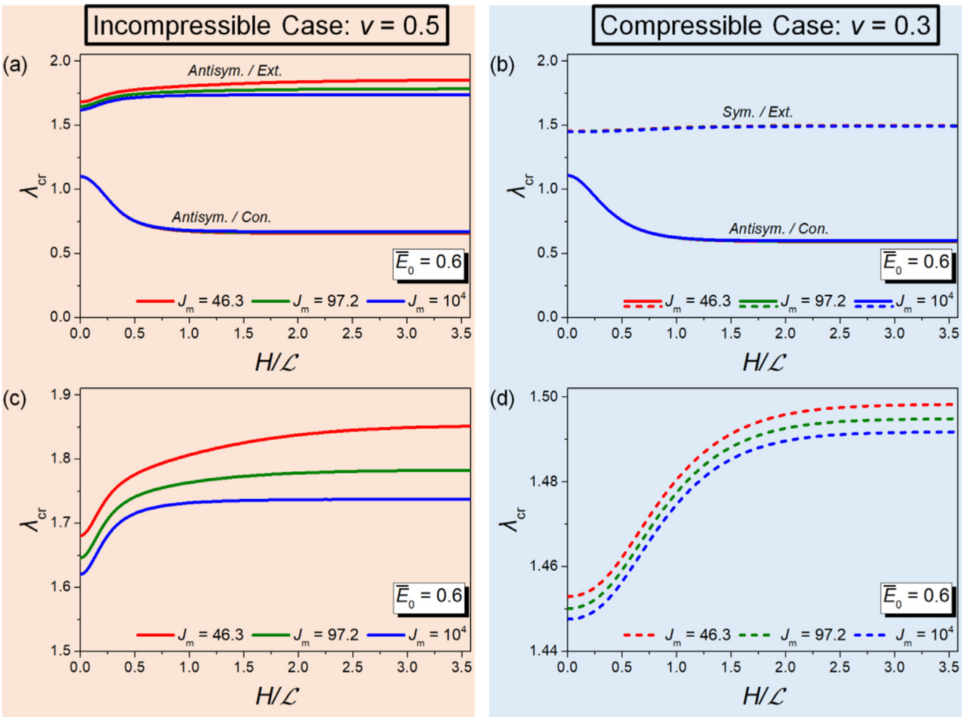

Fig. 4. Dispersion curves for incompressible and moderately compressible Gent ideal SEA plates with different chain extension limits ($J_m = 46.3, 97.2, 10^4$) subject to an equi-biaxial stretch and a constant bias voltage ($\bar{E}_0 = 0.6$): (a) $\nu = 0.5$; (b) $\nu = 0.3$. (c) and (d) provide locally enlarged details around the critical stretches of extensile wrinkling in (a) and (b), respectively. It shows that variation of the chain extension limit does not make a significant change in wrinkling in contraction, yet obvious influence on extensional wrinkling can be seen when the critical stretch is sufficiently close to the stiffening limit of tensile stretch. Here and below, "*Ext.*", "*Con.*" are used as the abbreviations of "extension" and "contraction", respectively.

(in the left column) and moderately compressible (in the right column) Gent ideal SEA plates with different chain extension limits, at a constant voltage $\bar{E}_0 = 0.6$ for illustration.

As expected, since the stiffening effect should only work in extension, the variations of chain extension limit do not make visible changes in contractile wrinkling where the critical stretches almost lie in the compressive regime, see, Figs. 4 (a, b). For the wrinkling in extension, as seen in Figs. 4 (c, d), the critical stretches increase as the chain extension limit decreases, indicating that the material stability can be enhanced by decreasing the stiffening parameter.

With the magnitude of critical stretches accounted, the results indicate that the effect of stiffening parameter monotonically decays as the critical stretches locate away from the stiffening limit of tensile stretch, or tensile limit for shorthand. It can thus explain why such effect is relatively obvious in incompressible SEA plates.

When referred to Fig. C5 or C6, one may note that significant variations in the critical stretches take place for symmetric wrinkling in contraction, which seems not consistent with the results above. Actually, it is because in this case the out-of-plane critical stretch, χ_{cr}, is very close to its tensile limit, thus the effect and mechanism revealed above also work well. In other words, the variations in-plane compressive critical stretches are due to the effect working on the out-of-plane tensile critical stretches.

2.3. Thin-plate and short-wave instabilities

In many scenarios, we may only concern the first encounter of wrinkling rather than specific wrinkling behaviors. When again referred to Figs. C1–C3, one may find that the stable region of the voltage-controlled plate is always located in between either the TPL or the SWL. Thus, an economic and efficient strategy based on the two extreme cases: thin-plate and short-wave instabilities is quite worthy of looking into. To this end, by virtue of Eqs. (1), (5) and (B33), we plot $\bar{E}_0 - \lambda$ curves in Fig. C7 to show the thin-plate and short-wave instabilities, together with a series of nonlinear loading curves and the onset of pull-in/snap-through, of the Gent ideal dielectric plates.

In the main text, we demonstrate the case of ν =0.3 as shown in Fig 5(a) with the unnecessary lines omitted. The black solid line corresponds to the short-wave instability. The thin-plate instability (blue solid line) is piecewise established, where the part between points C and D corresponds to the symmetric TPL while the rest belongs to the antisymmetric one. In this way, the stable region can be easily captured as the light green area.

Based on this, we can see that all the loading curves never enter the wrinkling region before the onset of pull-in instability (dotted line). Nevertheless, the critical value of the applied voltage for the onset of pull-in (marked by a black cross)

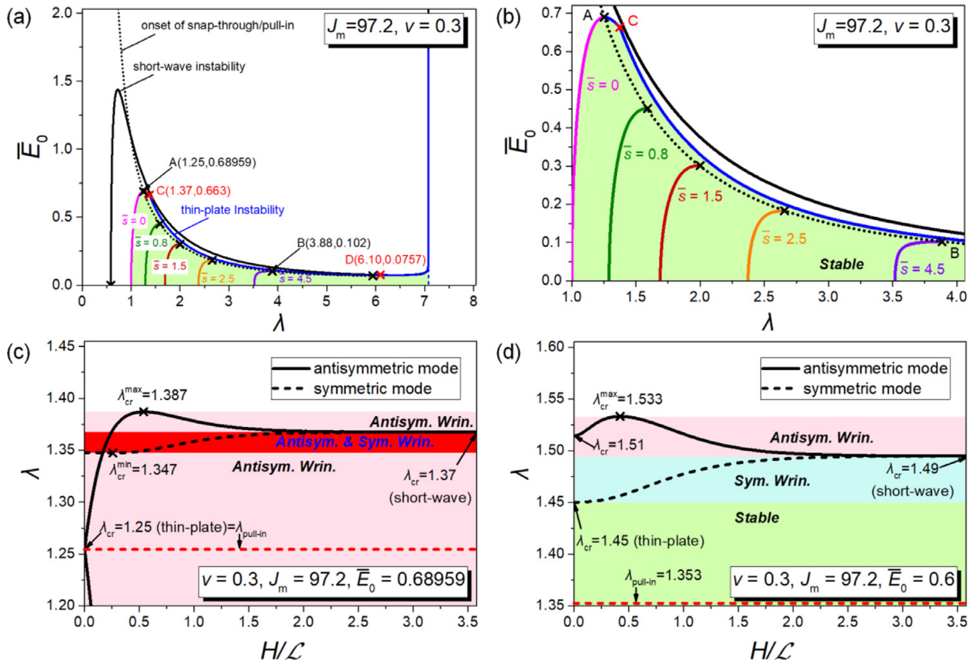

Fig. 5. Wrinkling emerges during the activation of pull-in: (a) thin-plate and short-wave instabilities along with loading curves of various pre-stresses ($\bar{s}$ =0, 0.8, 1.5, 2.5 and 4.5) for moderately compressible Gent ($\nu = 0.3$, $J_m = 97.2$) ideal SEA plates; (b) partial magnification of (a) shows that the onset of snap-through is quite close to the occurrence of thin-plate instability; phase diagrams of wrinkling instability for such SEA plates under diverse voltages: (c) $\bar{E}_0 = 0.68959$; and (d) $\bar{E}_0 = 0.6$. Note that the abbreviation of "*Antisym. & Sym. Wrin.*" is used to mark the range of stretch where wrinkling possibly occurs in either antisymmetric or symmetric mode.

is quite close to that for the thin-plate instability. Through a rescaled version as shown in Fig. 5(b), we can see that for the fixedly pre-stressed plate, the pull-in induced rapid expansion along the main faces is immediately followed by the occurrence of wrinkling. It can thus be used to explain the observation of wrinkles along with the pull-in as shown in Fig. 1(c), which has ever been implied in the incompressible problem (Su et al., 2018b).

We also reveal the role of compressibility in the correlation between these two types of instability. Taking the case of $\bar{s} = 0$ for example, the critical electric field for pull-in is approximately 0.69, of which the wrinkling behavior during the pull-in is established in Fig. 5(c). Unlike the incompressible plate where only one wrinkling mode, either symmetric or symmetric, can occur, both the two wrinkling modes can theoretically coexist in the compressible plate.

First, the wrinkling behaves in the antisymmetric mode at $\lambda \in [\sim 1.25, \sim 1.35]$ with a unique wave-length.

Then, it can be seen that the solid and dashed lines coexist in the highlighted red area, once the stretch reaches a critical value $\lambda \in [\sim 1.35, \sim 1.37]$, i.e., either symmetric or antisymmetric wrinkling may occur. Generally speaking, only one of them actually occurs in practice, which depends on the initial imperfection of the specific plate.

Finally, as the stretch rises beyond ~1.37, the plate simply wrinkles in the antisymmetric mode, which is almost immediately followed by electrical break-down (not displayed here).

Such pattern should hold for cases where the critical electric field of pull-in is located in the area above point C ($\bar{E}_0 =\sim 0.66$). For those where the critical electric field is located in the area between C and D, e.g., $\bar{s}$ =0.8, 1.5, 2.5, and 4.5, the cases get much simpler that the expanded plate first wrinkles symmetrically and then anti-symmetrically as the stretch increases, see, e.g., Fig. 5(d) for $\bar{E}_0 =\sim 0.6$. The reader may be referred to Figs. C7 and C8 for more details.

3. Charge-controlled compressible SEA plate

In this section, we examine the instability behaviors of compressible SEA plates actuated through spraying electric charges Q on the main faces, as shown in the right column of Fig. 2. It is so-called charge-controlled plate where the transverse nominal electric displacement can be obtained as $D_0 = Q/(L_1 L_2)$.

3.1. Nonlinear response

According to Eq. (A15), the nonlinear responses of Gent and neo-Hookean ideal SEA plates read

$$\bar{s} = \frac{\lambda\left(1 - \chi^2/\lambda^2\right)}{1 - (I_1 - 3)/J_m} - \bar{D}_0^2 \chi/\lambda^3, \bar{s} = \lambda\left(1 - \chi^2/\lambda^2\right) - \bar{D}_0^2 \chi/\lambda^3, \quad (7)$$

respectively, where $\bar{D}_0 = D_0/\sqrt{\mu\varepsilon}$ is a non-dimensional measure of D_0. It should be noted that no pull-in occurs in the current case for the lack of positive feedback mechanism as found in the voltage-controlled case.

3.2. Inhomogeneous and small-amplitude wrinkling

As the incremental boundary conditions adjust in the present problem, the Stroh vector becomes slightly different from that for the voltage-controlled case, resulting in a modified Stroh matrix as described in Appendix B.3.

We also consider the example of a neo-Hookean ideal SEA plate, for which the dispersion equation reads

$$\frac{\left(\bar{D}_3^2 + \frac{r_2 + r_2^{-1}}{\lambda}\right)^2}{(1 - r_2^2)/\lambda}\left[\frac{\coth(r_2\chi\pi H/\mathcal{L})}{\coth(\chi\pi H/\mathcal{L})}\right]^{\pm 1} - \frac{r_3\left(\bar{D}_3^2 + \frac{2}{r_2\lambda}\right)^2}{(r_2^{-1} - r_2)/\lambda}\left[\frac{\coth(r_3\chi\pi H/\mathcal{L})}{\coth(\chi\pi H/\mathcal{L})}\right]^{\pm 1} = \bar{D}_3^2, \tag{8}$$

where the definitions of r_2, and r_3 follow Eq. (3).

With the electrical actuation considered, the dispersion relation in terms of the prescribed nominal electric displacement is given as

$$\frac{\left[\bar{D}_0^2 + \lambda^3(r_2 + r_2^{-1})\right]^2}{\lambda^3(1 - r_2^2)}\left[\frac{\coth(r_2\chi\pi H/\mathcal{L})}{\coth(\chi\pi H/\mathcal{L})}\right]^{\pm 1} - \frac{r_3\left(\bar{D}_0^2 + \frac{2\lambda^3}{r_2}\right)^2}{\lambda^3(r_2^{-1} - r_2)}\left[\frac{\coth(r_3\chi\pi H/\mathcal{L})}{\coth(\chi\pi H/\mathcal{L})}\right]^{\pm 1} = \bar{D}_0^2, \tag{9}$$

where $r_3 = \sqrt{1 - (\chi^{-1} - \lambda^{-2}\chi)/[2(\lambda^{-4}\bar{D}_0^2 - 2J^3\bar{\Omega}_{33})]}$.

Accordingly, the equation for the short-wave limit reads

$$\frac{\left[\bar{D}_0^2 + \lambda^3(r_2 + r_2^{-1})\right]^2}{1 - r_2^2} - \frac{\left(\bar{D}_0^2 + 2\lambda^3 r_2^{-1}\right)^2 r_3}{r_2^{-1} - r_2} = \lambda^3\bar{D}_0^2. \tag{10}$$

The dispersion equations for the incompressible case can be obtained as

$$\left[\frac{\tanh(\lambda\pi H/\mathcal{L})}{\tanh(\lambda^{-2}\pi H/\mathcal{L})}\right]^{\pm 1} = \frac{\left(\bar{D}_0^2 + \lambda^6 + 1\right)^2}{\bar{D}_0^2\lambda^3(1 - \lambda^6) + \lambda^3\left(\bar{D}_0^2 + 2\right)^2}. \tag{11}$$

All these general relations have never been reported before; only some special cases have been discussed by Conroy Broderick et al. (2020).

3.2.1. Example: neo-Hookean ideal SEA plate

Our attention is now restricted to the slightly and moderately compressible neo-Hookean ideal SEA plates for studying their wrinkling behaviors, as shown in Fig. 6. For ease of discussion, we zoom in on the area around the border between the stable and wrinkled regions. Two considered plates are both sufficiently stretched to be stable originally, which can only wrinkles in contraction with the release of stretch.

For plates subject to a low electric displacement ($\bar{D}_0 = 4.0$), see, Figs. 6 (a, b), antisymmetric wrinkling always occurs prior to the symmetric one, regardless of the compressibility of the material. Specifically, the moderately compressible plate begins to wrinkle at the critical stretch of $\lambda_{cr} =\sim 1.56$ and the antisymmetric wrinkling vanishes once $\lambda <\sim 1.42$, while the antisymmetric wrinkling of the slightly compressible one emerges among $\lambda \in [\sim 1.58, \sim 1.41]$. It means that, stronger compressibility can not only suppress the onset of antisymmetric wrinkling but also compress its active region, which is quite in opposite to the voltage-controlled case as seen in Figs. C1–C3. When further referred to Figs. C9–C11, we find this feature is independent of the magnitude of electric stimuli.

Moreover, one may note that the symmetric dispersion curve in Fig. 6(b) mildly overlaps the antisymmetric one, thus generating an extremely narrow area, marked by a red band as enlarged in the inset of Fig. 6(b), between the regions of purely antisymmetric and symmetric wrinkling. In this band, the wrinkling of plate may occur in either antisymmetric or symmetric mode, and each mode possibly corresponds to more than one wave-length. It is similar to but even more complex than that shown in Fig. 5(c) for $\lambda \in [\sim 1.35, \sim 1.37]$. However, as this band is so narrow and not found in both incompressible and slightly compressible cases, a question rises that whether it is surely induced by the enhancement of compressibility.

We thus increase the biasing electric displacement up to 12.0 so as to further check the wrinkling behavior. As seen in Fig. 6(c) for the slightly compressible case, a similar but even wider band area emerges at $\lambda \in [\sim 2.16, \sim 2.18]$ as the symmetric dispersion curve also overlaps the antisymmetric one. For the moderately compressible case as shown in Fig. 6(d), the band shifts upward to be located in $\lambda \in [\sim 2.08, \sim 2.15]$ and becomes much wider than that in Fig. 6(c) for $\bar{D}_0 = 4.0$. In consideration of the fact that this band is absent in the incompressible case (e.g., Fig. C9), we can make sure that high electric biasing field cannot independently induce such phenomenon. Hence, the occurrence of such band area should only attribute to the promotion of symmetric wrinkling by the enhancing compressibility, upon which the increasing electric displacement strengthens it significantly.

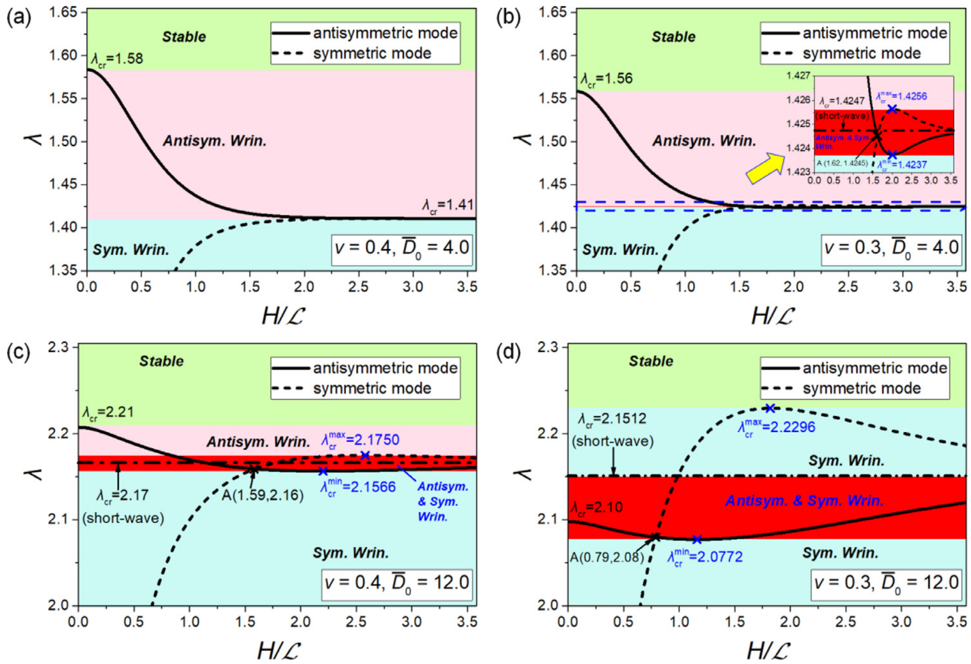

Fig. 6. Phase diagrams of wrinkling instability for equi-biaxially stretched charge-controlled neo-Hookean ideal SEA plates, where the black solid and dashed lines are the dispersion curves for the antisymmetric and symmetric wrinkles, respectively: (a) $\nu = 0.4$ and $\bar{D}_0 = 4.0$; (b) $\nu = 0.3$ and $\bar{D}_0 = 4.0$; (c) $\nu = 0.4$ and $\bar{D}_0 = 12.0$; (d) $\nu = 0.3$ and $\bar{D}_0 = 12.0$.

It is worth noting that the antisymmetric mode is in general the prior failure mode and dispersion curves are always monotonous in the incompressible case (Su et al., 2018b). However, for the considered problem, the purely antisymmetric wrinkling eventually vanishes in Fig. 6(d) due to the significant promotion of symmetric wrinkling and the critical stretch for the first encounter of wrinkling is ~2.23, even not at its TPL or SWL. Interestingly, though the antisymmetric wrinkling is much suppressed, see, $\lambda_{cr} =\sim 2.21$ in Fig. 6(c) and $\lambda_{cr} =\sim 2.15$ in Fig. 6(d), the moderately compressible plate is actually more susceptible to wrinkling than the slightly compressible one. In this sense, a competitive mechanism is proposed that the enhancement of compressibility facilitates the onset of symmetric wrinkling while suppresses the occurrence of antisymmetric one, which in principle determines the apparent wrinkling behavior of charge-controlled compressible SEA plates.

3.2.2. Example: Gent ideal dielectric plate

We then examine the effect of chain extension limit on the wrinkling of the charge-controlled plates. Fig. 7 presents the dispersion curves for the equi-biaxially stretched incompressible and moderately compressible plates with various chain extension limits. In the left column, we omit the curves for the symmetric mode since the incompressible plate always first wrinkles in the antisymmetric mode. The reader may be referred to Fig. C12 for complete plots. As seen in Fig. 7 (a, b) for $\bar{D}_0 = 4.0$, the differences between these dispersion curves are tiny but not that negligible as ever shown in Fig. 4. The effect of chain extension limit on wrinkling is monotonic that the plate with a smaller J_m always has a smaller critical stretch for any fixed $H/\mathcal{L}$, either in the antisymmetric or symmetric mode. When the electric displacement increases as shown in Fig. 7 (c, d) up to 12.0, it is found this effect gets more visible as the critical stretches gradually approach the tensile limit. It again verifies that the role of chain extension limit in wrinkling is localized and independent of electrical loading protocols.

3.3. Thin-plate and short-wave instabilities

Recalling Figs. C9 and C10, either charge-controlled incompressible or slightly compressible plate wrinkles first at either TPL or SWL. This rule only holds for moderately compressible plate under low electric biasing field, see, e.g., Fig. 6(b), yet a mild misestimation may occur for a high electric displacement, see, e.g., Fig. 6(d). Even so, we can see that the deviation for the latter case is located in a reasonable range, see, e.g., only ~−1.76% and ~−3.5% in Figs. C11 (c, d), respectively. Thus, thin-plate and short-wave instabilities are still of great significance for predicting the critical onset of wrinkling with a small allowance applied in practical use.

With the help of Eqs. (7), (10) and (B33), we plot the $\bar{D}_0 - \lambda$ curves for thin-plate and short-wave instabilities along with a series of loading curves for the neo-Hookean ideal SEA plates of different compressibility in Fig C13. Note that in this case these two instabilities are given by antisymmetric TPL and SWL, respectively.

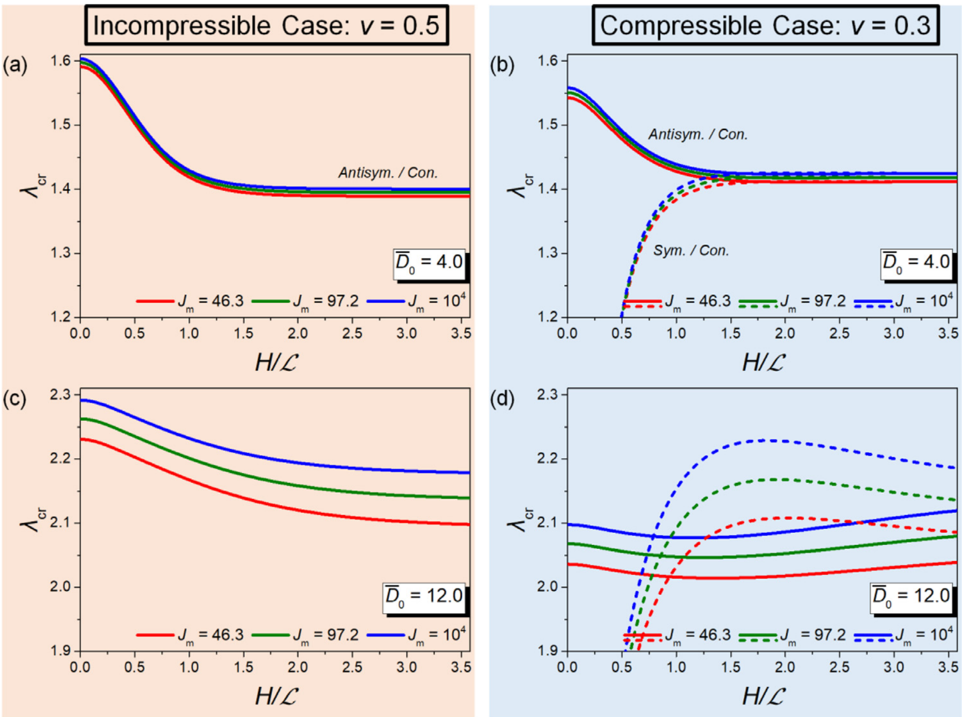

Fig. 7. Dispersion curves for equi-biaxially stretched incompressible and moderately compressible Gent ideal SEA plates of different chain extension limits (J_m =46.3, 97.2, 10^4) subject to constant charges sprayed on the main faces ($\bar{D}_0$ =4.0, and 12.0).

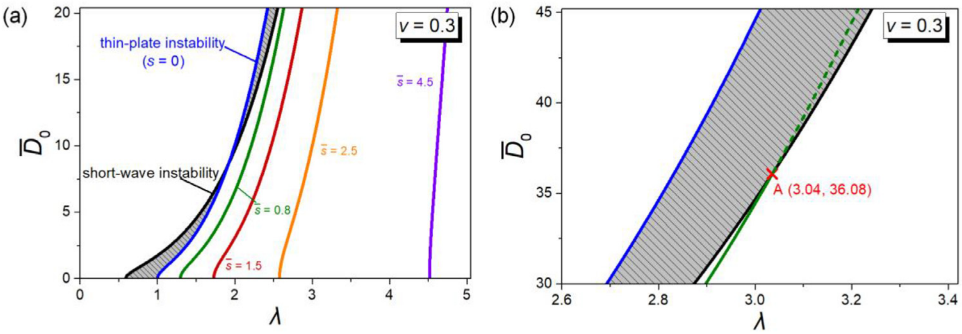

Fig. 8. How the wrinkling instability emerges in equi-biaxially loaded charge-controlled plates: (a) Thin-plate and short-wave instabilities along with loading curves of various pre-stresses ($\bar{s}$ =0, 0.8, 1.5, 2.5 and 4.5) for moderately compressible ($\nu = 0.3$) neo-Hookean ideal SEA plates; (b) the loading curve for $\bar{s} = 0.8$ get crossed with the curve for the SWLs when $\bar{D}_0$ reaches a sufficiently large value (>~36.08) and wrinkles rise if $\bar{D}_0$ keeps increasing.

First, it is reconfirmed in Fig. C13(a) for $\nu = 0.5$ that, no loading curve crosses the gray area between the TPL and SWL, which means wrinkling in extension does not take place (Conroy Broderick et al., 2020).

We then move to the slightly ($\nu = 0.4$) and moderately ($\nu = 0.3$) compressible cases in Figs. C13 (b, c). In contrast to the incompressible case, the TPL gets crossed with the SWL as soon as $\bar{D}_0$ reaches a certain value. That is, a compressible charge-controlled SEA plate, such as the SEA plate considered here, without in-plane pre-stress is not always geometrically stable.

Finally, we focus on the moderately compressible case with Fig. C13(c) rearranged in Fig. 8. As shown in Fig. 8(a), when $\bar{D}_0$ is located in a small scale, all the loading curves do not cross the gray region between the TPL and SWL. As the pre-stress increases, the loading curve successively gets away from this region, which suggests that the stability may be significantly improved by increasing the in-plane pre-stress.

Nevertheless, for a sufficiently large $\bar{D}_0$, see, e.g., the insert of Fig. C13(c), the loading curve for $\bar{s} = 0.8$ (in olive) will eventually cross the SWL. In Fig. 8(b) we provide an enlarged version of the area around the intersection, denoted by A. It is noted that the actual onset of instability in this case should be a bit larger than the SWL as underlined above, thus this slightly pre-stressed plate wrinkles a bit prior to A.

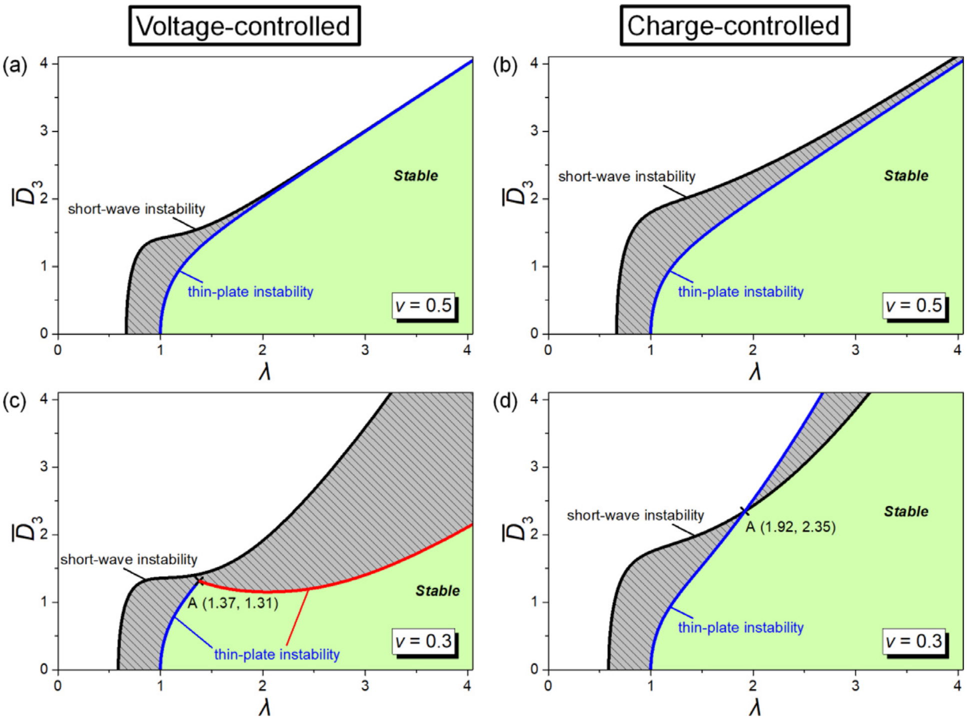

Fig. 9. Comparison of wrinkling instability between equi-biaxially stretched voltage- and charge-controlled neo-Hookean ideal SEA plates. The moderately compressible plate under the charge-controlled condition is much more stable than that under the voltage-controlled condition while the intrinsic instability of the incompressible plate is independent of the electric loading protocol.

4. Electric-induced intrinsic instability

In the above sections, wrinkling instability is expressed by the critical stretch with either nominal electric field or nominal electric displacement. These nominal quantities are usually easy to measure and thus preferred in practical situations. However, one critical issue emerges that how the wrinkling behaves during the switch between different electrical actuations. Here, we introduce the so-called intrinsic instability as ever done in the problem of half-space (Dorfmann & Ogden, 2014; Xia et al., 2020). The word "intrinsic" reflects the fact that the onset of instability is only correlated to the true electric variables. If the whole theoretical framework is constructed in terms of the true electric displacement, then it can be specifically applied with respect to the nominal electrical variables by using a pull-back operation.

As illustration, we compare the intrinsic TPL and SWL of the incompressible and moderately compressible neo-Hookean ideal SEA plates in Fig. 9, where the black and blue lines correspond to short-wave and thin-plate instabilities, respectively. We first see in Fig. 9 (a, b) that the short-wave instability of the charge-controlled incompressible plate is located above that of the voltage-controlled plate, which is exactly in line with the results for the electroactive half-space (i.e., $H \to \infty$) (Xia et al., 2020). It means that the charge-controlled plate is more stable than the voltage-controlled one when the initial thickness is very large. As $H \to 0$, the critical curve for either case approaches the thin-plate instability, which corresponds to the antisymmetric mode governed by Eq. (B33). One may note that, as the stable regions (colored in light green) here are solely determined by such thin-plate instability, the intrinsic instability of the incompressible SEA plate with finite thickness is actually independent of the electrical loading protocol. It is also supported by a direct comparison in Fig. C13(a), and as expected, all these extreme cases become essentially identical when $\bar{D}$ is sufficiently large, see, Fig. C13(b).

For the moderately compressible plate, when compared with the incompressible case, as seen in Fig. 9 (c, d), while the thick plate (or half-space) is also more liable to loss of stability subject to the voltage-controlled actuation, the intrinsic instability for the case of finite thickness does not only depend on the antisymmetric TPL.

For a voltage-controlled extremely thin plate, see Fig. 9(c) or C.14(e), the wrinkling first occurs in the antisymmetric mode when the critical stretch is located between 1 and ~1.37 and then mutates into symmetric mode as soon as the critical stretch increases beyond ~1.37. In Fig. 9(d) for the charge-controlled plate, the thin-plate instability may enter the area above the short-wave instability with an intersection of (~1.92, ~2.35). As so, the wrinkling is first encountered at the antisymmetric TPL when $0 \leq \bar{D} <\sim 2.35$ and then at the SWL once $\bar{D} >\sim 2.35$.

Through a direct comparison between the stable regions as presented in Fig. 9 (c, d), we can see that, the charge-controlled case has a much larger stable region thus possessing much better intrinsic stability than the voltage-controlled case. When further considering Fig. C14, we find that, as the compressibility gradually increases ($\nu : 0.5 \to 0.4 \to 0.3$), the stable region of the voltage-controlled plate shrinks, see, Figs. C14 (a, c, e), while that of the charge-controlled plate expands, see, Figs. C14 (a, d, f) instead. Since the real SEA materials are always to some extent compressible, we may well tune their wrinkling instability by switching the electrical loading protocols, similar to the case of pull-in instability. Zhang, Zhao, Wang, Chen, and Li (2017) recently proposed that a combination of voltage- and charge-control is feasible for guaranteeing a large deformation of DE without electromechanical instability. In this sense, such way may also be useful for realizing large deformations of SEA materials with a low risk of wrinkling instability.

5. Conclusions

We propose a general analysis for surface instability of *compressible* soft electroactive plates by using the surface impedance matrix method with Stroh formulation. As an illustration, a series of analytical dispersion relations are derived for the electric-induced wrinkling of equi-biaxially stretched generalized ideal SEA plates. The expressions are given in matrix forms thus are easy for programming in commercial algebraic software, such as MATLAB, Mathematica, etc.

The results reveal some unique and significant effects of material compressibility on the wrinkling behaviors:

(1) For the voltage-controlled problem, the stability of plate gets monotonically deteriorated with the increase of compressibility, where the wrinkling in extension (if exists) may appear in the symmetric mode prior to the antisymmetric mode;
(2) For the charge-controlled problem, an interesting competition mechanism accounting for the encounter of wrinkling is revealed that the antisymmetric wrinkling is suppressed while the symmetric one is promoted by the release of incompressibility constraint;
(3) the electric biasing field always plays a role of positive gain factor for facilitating the effects stated in (1) and (2).

On the other hand, in both cases, the plate with a smaller chain extension limit always poses better stability. In particular, with the decrease of Poisson's ratio, this negative correlation is gradually impaired in the voltage-controlled plate while no visible variation is found in the charge-controlled one. It can be uniformly explained by that such effect is localized and quickly decays as the critical stretches get far away from the stiffening limit of tensile stretch of the plate.

The thin-plate and short-wave limits can be utilized to exactly define the stability of the voltage-controlled plate while proper (usually small) modification is required for the use in the charge-controlled plate. Moreover, for the latter case, the plate under dead-loads may not always keep geometrically stable as its compressibility increases.

Most interestingly, with the electrical independence of the intrinsic instability understood in the incompressible case, such instability of the charge-controlled plate is found improved with the increase of compressibility while that of the voltage-controlled plate worsens instead. It indeed indicates a better electrical safety of the charge-controlled actuation.

As such, the analysis provides a pragmatic and maneuverable strategy to predict the surface instability among a wide range of SEA-based devices. Surely, there are other causes, such as lateral boundary conditions, possible dissipation and actual electrical inhomogeneity, also responsible for the actual loss of stability. They should be interesting and will be discussed in the near future.

Finally, it is pointed out that, although the numerical calculations are performed for the voltage- and charge-controlled plates in cases of Gent and neo-Hookean ideal dielectrics, the method can be easily extended to the case of an SEA material characterized by the Mooney-Rivlin, Ogden or Arruda–Boyce model (Boyce & Arruda, 2000).

Declaration of Competing Interest

The authors declare that they have no known competing financial interests or personal relationships that could have appeared to influence the work reported in this paper.

Acknowledgments

The work was supported by the Natural Science Foundation of Zhejiang Province, China (No. LD21A020001) and the National Natural Science Foundation of China (No. 11872329). Partial supports from Wenzhou City Huang Mengqi Dandelion Charitable Foundation, and 2019 Zhejiang University Academic Award for Outstanding Doctoral Candidates are also acknowledged.

Appendix A. Preliminaries of the theoretical framework

In this part, we briefly recall the nonlinear continuum theory for SEA materials and its incremental version. The appendix is self-contained and some equations from the main text will be repeated.

A.1. Theory of nonlinear electroelasticity

An SEA body is assumed to originally occupy a region, $\mathcal{B}_0$, with boundary, $\partial\mathcal{B}_0$, in the undistorted reference configuration, where any material point in $\mathcal{B}_0$ is denoted by its position vector, X. Subject to mechanical stretches and electrical stimuli, the material points in the body will move to a new position, x, such that the body occupies a new region, B, with new boundary, ∂B, referred to as the current configuration. This process may be described by a deformation gradient, $\boldsymbol{F} = \partial\boldsymbol{x}/\partial\boldsymbol{X}$, and the variation of local volume reads $J = \det\boldsymbol{F}$. We may thus write the left and right Cauchy-Green tensors as $\boldsymbol{b} = \boldsymbol{F}\boldsymbol{F}^T$ and $\boldsymbol{c} = \boldsymbol{F}^T\boldsymbol{F}$, respectively, where the superscript T denotes transpose.

We now introduce a free energy density function, $\Omega(\boldsymbol{F}, \boldsymbol{D}_1)$, satisfying $\Omega(\boldsymbol{I}, \boldsymbol{0}) = 0$. In this function, I is the identity tensor for undeformed state, and $\boldsymbol{D}_l$ is the nominal electric displacement. Then, the nonlinear constitutive relations read

$$\boldsymbol{T} = \frac{\partial\Omega}{\partial\boldsymbol{F}}, \quad \boldsymbol{E}_1 = \frac{\partial\Omega}{\partial\boldsymbol{D}_1}, \tag{A1}$$

where the nominal stress tensor $\boldsymbol{T} = J\boldsymbol{F}^{-1}\boldsymbol{\tau}$ and the nominal electric field $\boldsymbol{E}_l = \boldsymbol{F}^{\mathrm{T}}\boldsymbol{E}$ are the pull-back versions of the total Cauchy stress τ and the true electric field E.

For general isotropic SEA materials, we have

$$\begin{aligned} J\boldsymbol{\tau} &= 2\Omega_1\boldsymbol{b} + 2\Omega_2\left(I_1\boldsymbol{b} - \boldsymbol{b}^2\right) + 2I_3\Omega_3\boldsymbol{I} + 2J^2\Omega_5\boldsymbol{D}\otimes\boldsymbol{D} \\ &\quad + 2\Omega_6 J^2(\boldsymbol{D}\otimes\boldsymbol{b}\boldsymbol{D} + \boldsymbol{b}\boldsymbol{D}\otimes\boldsymbol{D}), \\ J\tau_{ji} &= 2\Omega_1 b_{ji} + 2\Omega_2\left(I_1 b_{ji} - b_{jk}b_{ki}\right) + 2\Omega_3 I_3\delta_{ji} + 2J^2\Omega_5 D_j D_i \\ &\quad + 2\Omega_6 J^2\left(D_j \mathrm{b}_{ik} D_{\mathrm{k}} + b_{jk}D_k D_i\right), \\ \boldsymbol{E} &= 2J\left(\Omega_4\boldsymbol{b}^{-1}\boldsymbol{D} + \Omega_5\boldsymbol{D} + \Omega_6\boldsymbol{b}\boldsymbol{D}\right), \\ \boldsymbol{E}_k &= 2J\left(\Omega_4 b_{ki}^{-1}D_i + \Omega_5 D_k + \Omega_6 b_{ik}D_i\right), \end{aligned} \tag{A2}$$

where $i,\ j,\ k = 1,\ 2,\ 3$, $\Omega_m = \partial\Omega/\partial I_m (m = 1, 2, \ldots, 6)$, the true electric displacement, D, is correlated with the nominal one by $\boldsymbol{D} = J^{-1}\boldsymbol{F}\boldsymbol{D}_1$, and $I_1 = \mathrm{tr}\boldsymbol{c}$, $I_2 = [(\mathrm{tr}\mathbf{c})^2 - \mathrm{tr}(\boldsymbol{c}^2)]/2$, $I_3 = \det\boldsymbol{c}$, $I_4 = \boldsymbol{D}_1\cdot\boldsymbol{D}_1$, $I_5 = \boldsymbol{D}_1\cdot(\boldsymbol{c}\boldsymbol{D}_1)$, $I_6 = \boldsymbol{D}_1\cdot(\boldsymbol{c}^2\boldsymbol{D}_1)$ are the six independent invariants for isotropic SEA materials.

The general constitutive relations in Eq. (A2) are rather lengthy, but it can be simplified quite a lot for some special forms of the free energy density. Hence, we further introduce the so-called generalized ideal dielectrics with the free energy density in the form

$$\Omega = W(I_1, I_3) + \frac{I_5}{2\varepsilon\sqrt{I_3}}, \tag{A3}$$

where W is an arbitrary purely elastic energy density function, only correlated to I_1 and I_3, and ε is the dielectric permittivity (in F/m). Especially, for the well-known compressible Gent (Gent, 1996; Horgan & Saccomandi, 2004) and neo-Hookean (Holzapfel, 2000; Xia et al., 2020) ideal dielectrics, we have

$$\begin{cases} W_{\mathrm{G}} = -\mu\left\{J_{\mathrm{m}}\ln\left[1 - (I_1 - 3)/J_{\mathrm{m}}\right] - \left(I_3^{-\beta} - 1\right)/\beta\right\}/2, \\ W_{\mathrm{nH}} = \mu\left[(I_1 - 3) + \left(I_3^{-\kappa} - 1\right)/\kappa\right]/2, \end{cases} \tag{A4}$$

where $\beta = \nu/(1 - 2\nu) - 1/J_{\mathrm{m}}$, $\kappa = \nu/(1 - 2\nu)$, μ and ν are the initial shear modulus (in Pa) and Poisson's ratio (dimensionless) of the material, respectively, and J_{m} is the maximum allowed for $I_1 - 3$, which is also referred to as the dimensionless stiffening parameter or chain extension limit. One may note that, as $J_{\mathrm{m}} \to \infty$, the Gent model reduces to the neo-Hookean model, where $\kappa = \lim_{J_{\mathrm{m}}\to\infty}\beta$.

As shown in Fig. 2(a), we then consider an SEA plate initially with thickness of H and length of L_1 and L_2 in the x_1- and x_2-directions, respectively. When applied with an arbitrary loading protocol described in Figs. 2 (b-g), the homogenous deformation and true electric displacement of the plate read

$$\boldsymbol{F} = \mathrm{diag}(\lambda_1, \lambda_2, \chi), \quad \boldsymbol{D} = [0, 0, D_3]^T, \tag{A5}$$

where λ_1 and λ_2 are the principal stretches along the x_1- and x_2- directions, respectively, and χ and D_3 are the principal stretch and the only nonzero component of the true electric displacement across the thickness, respectively. Note that we take $\lambda_1 = \lambda_2 = \lambda$ for the equi-biaxially stretched plate in the main text, yet λ_1 and λ_2 is in fact not necessarily identical in our general analysis.

Combining Eqs. (A2) and (A3), we obtain the following simplified expressions for the nonlinear responses and electric field of the material in the push-forward versions as

$$\begin{aligned} \tau_{11} &= \frac{2\lambda_1\Omega_1}{\lambda_2\chi} + 2J\Omega_3,\ \tau_{22} = \frac{2\lambda_2\Omega_1}{\lambda_1\chi} + 2J\Omega_3, \\ \tau_{33} &= \frac{2\chi\Omega_1}{\lambda_1\lambda_2} + 2J\Omega_3 + D_3^2/\varepsilon,\ E_3 = D_3/\varepsilon, \end{aligned} \tag{A6}$$

where E_3 is the only nonzero component of the true electric field. Note that the relationship between the nominal electric field and the electric displacement can be established as $D_3 = \varepsilon E_{l3}/\chi$.

For the plate with no mechanical traction applied on the main faces ($x_3 = \pm h/2$), as shown in Figs. 2 (b-g), we find the following compact expression for the in-plane stress components required to maintain the deformation as

$$\tau_{ii} = 2\left(\lambda_i^2 - \chi^2\right)\Omega_1/J - D_3^2/\varepsilon, \quad (i = 1, 2, \textit{ and no sum over } i) \tag{A7}$$

with the corresponding pull-back versions:

$$T_{\alpha i} = 2\left(\lambda_i^2 - \chi^2\right)\Omega_1/\lambda_i - JD_3^2/(\varepsilon\lambda_i), \tag{A8}$$

where the Roman and Greek subscripts correspond to the current and reference configurations, respectively.

For simplicity, we employ the following nondimensional quantities:

$$\begin{aligned}&\bar{W} = W/\mu, \bar{\boldsymbol{\tau}} = \boldsymbol{\tau}/\mu, \bar{\boldsymbol{D}} = \boldsymbol{D}/\sqrt{\mu\varepsilon}, \bar{\boldsymbol{E}} = \boldsymbol{E}/\sqrt{\mu/\varepsilon},\\ &\bar{I}_5 = I_5/(\mu\varepsilon), \bar{\mathbf{T}} = \mathbf{T}/\mu, \bar{\boldsymbol{D}}_l = \boldsymbol{D}_l/\sqrt{\mu\varepsilon}, \bar{\boldsymbol{E}}_l = \boldsymbol{E}_l/\sqrt{\mu/\varepsilon}.\end{aligned} \tag{A9}$$

Then we can rewrite Eqs. (A7) and (A8) in their nondimensional forms:

$$\bar{\tau}_{ii} = 2\left(\lambda_i^2 - \chi^2\right)\bar{W}_1/J - \bar{D}_3^2, \tag{A10}$$

and

$$\bar{T}_{\alpha i} = 2\left(\lambda_i^2 - \chi^2\right)\bar{W}_1/\lambda_i - J\bar{D}_3^2/\lambda_i, \tag{A11}$$

where $\bar{W}_1 \triangleq \partial\bar{W}/\partial I_1$ and $\bar{D}_3 = D_3/\sqrt{\mu\varepsilon}$ is a non-dimensional measurement of D_3.

For given nominal electric field (*voltage-controlled problem*), we rewrite Eqs. (A10) and (A11) by using the relationship $\bar{D}_3 = \bar{E}_{l3}/\chi$ as

$$\bar{\tau}_{ii} = 2\left(\lambda_i^2 - \chi^2\right)\bar{W}_1/J - \bar{E}_{l3}^2/\chi^2, \tag{A12}$$

and

$$\bar{T}_{\alpha i} = 2\left(\lambda_i^2 - \chi^2\right)\bar{W}_1/\lambda_i - J\bar{E}_{l3}^2/\left(\lambda_i\chi^2\right). \tag{A13}$$

For given nominal electric displacement (*charge-controlled problem*), we rewrite Eqs. (A10) and (A11) by using the relationship $\bar{D}_3 = J^{-1}\chi\bar{D}_{l3}$ as

$$\bar{\tau}_{ii} = 2\left(\lambda_i^2 - \chi^2\right)\bar{W}_1/J - J^{-2}\chi^2\bar{D}_{l3}^2, \tag{A14}$$

and

$$\bar{T}_{\alpha i} = 2\left(\lambda_i^2 - \chi^2\right)\bar{W}_1/\lambda_i - J^{-1}\chi^2\bar{D}_{l3}^2/\lambda_i. \tag{A15}$$

A.2. Linearized incremental theory

Upon the deformed configuration, we superpose an arbitrary infinitesimal perturbation to produce an incremental field. Hereinafter, all incremental quantities will be represented by the dotted variables. In this manner, we write the Eulerian forms of equilibrium equations of the incremental motion as

$$\mathrm{div}\dot{\boldsymbol{T}}_0 = \mathbf{0}, \quad \mathrm{div}\ \dot{\boldsymbol{D}}_{l0} = 0, \quad \mathrm{curl}\ \dot{\boldsymbol{E}}_{l0} = \mathbf{0}, \tag{A16}$$

where $\dot{\boldsymbol{T}}_0$, $\dot{\boldsymbol{D}}_{l0}$ and $\dot{\boldsymbol{E}}_{l0}$ are the push-forward versions of the incremental stress, electric displacement, and electric field, respectively. The incremental constitutive relations read

$$\dot{\boldsymbol{T}}_0 = \mathcal{A}_0\boldsymbol{H} + \boldsymbol{\Gamma}_0\dot{\boldsymbol{D}}_{l0}, \qquad \dot{\boldsymbol{E}}_{l0} = \boldsymbol{\Gamma}_0^T\boldsymbol{H} + \boldsymbol{K}_0\dot{\boldsymbol{D}}_{l0}, \tag{A17}$$

where $\boldsymbol{H} = \mathrm{grad}\,\boldsymbol{u}$ is the displacement gradient with respect to $\boldsymbol{x}, \boldsymbol{u}$ is the incremental displacement vector, and $\mathcal{A}_0$, $\boldsymbol{\Gamma}_0$ and $\boldsymbol{K}_0$ are the fourth-, third-, and second-order effective material tensors, respectively, with the following component forms

$$\begin{aligned}
\mathcal{A}_{0jilk} &= \mathcal{A}_{0jilk}^{(0)} + \mathcal{A}_{0jilk}^{(1)} + \mathcal{A}_{0jilk}^{(2)} + \mathcal{A}_{0jilk}^{(3)} + \mathcal{A}_{0jilk}^{(4)} = \mathcal{A}_{0lkji},\\
\mathcal{A}_{0jilk}^{(0)} &= 4J^{-1}\left[\Omega_{11}b_{ji}b_{lk} + \Omega_{22}\left(I_1b_{ji} - b_{jm}b_{im}\right)(I_1b_{lk} - b_{ln}b_{kn})\right]\\
&\quad + 4J^3\left[\Omega_{33}\delta_{ji}\delta_{lk} + \Omega_{55}D_jD_iD_lD_k + \Omega_{66}\left(b_{jm}D_mD_i + D_jb_{im}D_m\right)(b_{ln}D_nD_k + D_lb_{kn}D_n)\right],\\
\mathcal{A}_{0jilk}^{(1)} &= 4J^{-1}\Omega_{12}\left[b_{ji}(I_1b_{lk} - b_{ln}b_{kn}) + b_{lk}\left(I_1b_{ji} - b_{jm}b_{im}\right)\right]\\
&\quad + 4J\begin{Bmatrix}\Omega_{13}\left(b_{ji}\delta_{lk} + b_{lk}\delta_{ji}\right) + \Omega_{15}\left(b_{ji}D_lD_k + b_{lk}D_jD_i\right)\\ +\Omega_{16}\left[b_{ji}(b_{ln}D_nD_k + D_lb_{kn}D_n) + b_{lk}\left(b_{jm}D_mD_i + D_jb_{im}D_m\right)\right]\end{Bmatrix},\\
\mathcal{A}_{0jilk}^{(2)} &= 4J\begin{Bmatrix}\Omega_{23}\left[\left(I_1b_{ji} - b_{jm}b_{im}\right)\delta_{lk} + (I_1b_{lk} - b_{ln}b_{kn})\delta_{ji}\right]\\ +\Omega_{25}\left[D_jD_i(I_1b_{lk} - b_{ln}b_{kn}) + D_lD_k\left(I_1b_{ji} - b_{jm}b_{im}\right)\right]\\ +\Omega_{26}\left[\left(I_1b_{ji} - b_{jm}b_{im}\right)(b_{ln}D_nD_k + D_lb_{kn}D_n) + \left(b_{jm}D_mD_i + D_jb_{im}D_m\right)(I_1b_{lk} - b_{ln}b_{kn})\right]\end{Bmatrix},
\end{aligned}$$

$$\mathcal{A}^{(3)}_{0jilk} = 4J^3\left\{\begin{array}{l}\Omega_{35}\left(\delta_{ji}D_lD_k + \delta_{lk}D_jD_i\right)\\ +\Omega_{36}\left[\delta_{ji}(b_{ln}D_nD_k + D_lb_{kn}D_n) + \delta_{lk}\left(b_{jm}D_mD_i + D_jb_{im}D_m\right)\right]\\ +\Omega_{56}\left[D_jD_i(b_{ln}D_nD_k + D_lb_{kn}D_n) + D_lD_k\left(b_{jm}D_mD_i + D_jb_{im}D_m\right)\right]\end{array}\right\},$$

$$\begin{aligned}\mathcal{A}^{(4)}_{0jilk} = {}& 2J^{-1}\left[\Omega_1 b_{jl}\delta_{ik} + \Omega_2\left(2b_{ji}b_{lk} - b_{jl}b_{ik} - b_{jk}b_{li} + I_1b_{jl}\delta_{ik} - b_{jm}b_{lm}\delta_{ik}\right)\right]\\ & + 2J\left[\begin{array}{l}\Omega_3\left(2\delta_{ji}\delta_{lk} - \delta_{jk}\delta_{li}\right) + \Omega_5 D_jD_l\delta_{ik}\\ +\Omega_6\begin{pmatrix}b_{jk}D_lD_i + b_{li}D_jD_k + b_{jl}D_iD_k\\ +b_{ik}D_jD_l + b_{jm}D_m\delta_{ik}D_l + b_{ln}D_n\delta_{ik}D_j\end{pmatrix}\end{array}\right],\end{aligned}\tag{A18}$$

$$\begin{aligned}&\Gamma_{0jik} = \Gamma^{(1)}_{0jik} + \Gamma^{(2)}_{0jik} + \Gamma^{(3)}_{0jik} + \Gamma^{(4)}_{0jik} + \Gamma^{(5)}_{0jik} + \Gamma^{(6)}_{0jik} = \Gamma_{0ijk},\\ &\Gamma^{(1)}_{0jik} = 4Jb_{ji}\left(\Omega_{14}b^{-1}_{kn}D_n + \Omega_{15}D_k + \Omega_{16}b_{kn}D_n\right),\\ &\Gamma^{(2)}_{0jik} = 4J\left(I_1b_{ji} - b_{jm}b_{mi}\right)\left(\Omega_{24}b^{-1}_{kn}D_n + \Omega_{25}D_k + \Omega_{26}b_{kn}D_n\right),\\ &\Gamma^{(3)}_{0jik} = 4J^3\delta_{ji}\left(\Omega_{34}b^{-1}_{kn}D_n + \Omega_{35}D_k + \Omega_{36}b_{kn}D_n\right),\\ &\Gamma^{(4)}_{0jik} = 4J^3\left\{\begin{array}{l}b^{-1}_{kn}D_n\left[\Omega_{45}D_jD_i + \Omega_{46}\left(b_{jm}D_mD_i + b_{im}D_mD_j\right)\right]\\ +\Omega_{56}\left[D_jD_ib_{kn}D_n + \left(b_{jm}D_mD_i + b_{im}D_mD_j\right)D_k\right]\end{array}\right\},\\ &\Gamma^{(5)}_{0jik} = 4J^3\left[\Omega_{55}D_jD_iD_k + \Omega_{66}\left(b_{jm}D_mD_i + b_{im}D_mD_j\right)b_{kn}D_n\right],\\ &\Gamma^{(6)}_{0jik} = 2J\Omega_5\left(D_i\delta_{jk} + D_j\delta_{ik}\right) + 2J\Omega_6\left(b_{jk}D_i + b_{ik}D_j + b_{jm}D_m\delta_{ik} + b_{im}D_m\delta_{jk}\right),\end{aligned}\tag{A19}$$

$$\begin{aligned}&K_{0jk} = K^{(0)}_{0jk} + K^{(1)}_{0jk} + K^{(2)}_{0jk} = K_{0kj},\\ &K^{(0)}_{0jk} = 4J^3\left(\Omega_{44}b^{-1}_{jm}D_mb^{-1}_{kn}D_n + \Omega_{55}D_jD_k + \Omega_{66}b_{jn}D_nb_{km}D_m\right),\\ &K^{(1)}_{0jk} = 4J^3\left[\begin{array}{l}\Omega_{45}\left(b^{-1}_{jm}D_mD_k + b^{-1}_{kn}D_nD_j\right) + \Omega_{46}\left(b^{-1}_{jm}D_mb_{kn}D_n + b^{-1}_{kn}D_nb_{jm}D_m\right)\\ +\Omega_{56}\left(b_{jm}D_mD_k + b_{kn}D_nD_j\right)\end{array}\right],\\ &K^{(2)}_{0jk} = 2J\left(\Omega_4b^{-1}_{jk} + \Omega_5\delta_{jk} + \Omega_6b_{jk}\right),\quad (i,j,k,l = 1,2,3)\end{aligned}\tag{A20}$$

where b_{ji}, b_{lk}, ... are components of the left Cauchy-Green tensor, $\Omega_{mn} = \partial^2\Omega/(\partial I_m\partial I_n)$, $(m, n = 1, 2, ..., 6)$. Hereinafter, the Einstein summation convention always holds unless otherwise stated.

One may note that the following non-zero derivations of invariants with respect to the deformation gradient, F, and to the nominal electric displacement, $\boldsymbol{D}_l$, are applied impliedly

$$\begin{aligned}&\frac{\partial I_1}{\partial \boldsymbol{F}} = 2\boldsymbol{F}^{\mathrm{T}};\ \left(\frac{\partial I_1}{\partial \boldsymbol{F}}\right)_{\alpha i} = 2F_{i\alpha},\ \frac{\partial I_2}{\partial \boldsymbol{F}} = 2I_1\boldsymbol{F}^{\mathrm{T}} - 2\boldsymbol{F}^{\mathrm{T}}\boldsymbol{b};\ \left(\frac{\partial I_2}{\partial \boldsymbol{F}}\right)_{\alpha i} = 2I_1F_{i\alpha} - 2F_{m\alpha}b_{mi},\\ &\frac{\partial I_3}{\partial \boldsymbol{F}} = 2I_3\boldsymbol{F}^{-1};\ \left(\frac{\partial I_3}{\partial \boldsymbol{F}}\right)_{\alpha i} = 2I_3F^{-1}_{\alpha i},\ \frac{\partial I_5}{\partial \boldsymbol{F}} = 2I_3\boldsymbol{F}^{-1}\boldsymbol{D}\otimes\boldsymbol{D};\ \left(\frac{\partial I_5}{\partial \boldsymbol{F}}\right)_{\alpha i} = 2I_3F^{-1}_{\alpha m}D_mD_i,\\ &\frac{\partial I_6}{\partial \boldsymbol{F}} = 2J\left(J\boldsymbol{F}^{\mathrm{T}}\boldsymbol{D}\otimes\boldsymbol{D} + \boldsymbol{D}_l\otimes\boldsymbol{bD}\right);\ \left(\frac{\partial I_6}{\partial \boldsymbol{F}}\right)_{\alpha i} = 2J(JF_{m\alpha}D_mD_i + D_{l\alpha}B_{im}D_m),\end{aligned}\tag{A21}$$

$$\begin{aligned}&\frac{\partial I_4}{\partial \boldsymbol{D}_l} = 2\boldsymbol{D}_l;\ \left(\frac{\partial I_4}{\partial \boldsymbol{D}_l}\right)_{\alpha} = 2D_{l\alpha},\ \frac{\partial I_5}{\partial \boldsymbol{D}_l} = 2J\boldsymbol{F}^{\mathrm{T}}\boldsymbol{D};\ \left(\frac{\partial I_5}{\partial \boldsymbol{D}_l}\right)_{\alpha} = 2JF_{m\alpha}D_m,\\ &\frac{\partial I_6}{\partial \boldsymbol{D}_l} = 2J\boldsymbol{F}^{\mathrm{T}}\boldsymbol{bD};\ \left(\frac{\partial I_6}{\partial \boldsymbol{D}_l}\right)_{\alpha} = 2JF_{m\alpha}b_{mn}D_n,\end{aligned}\tag{A22}$$

$$\begin{aligned}&\frac{\partial^2 I_1}{\partial \boldsymbol{F}^2} = 2\delta_{ik}\delta_{\alpha\beta}\vec{\mathbf{e}}_\alpha\otimes\vec{\mathbf{e}}_i\otimes\vec{\mathbf{e}}_\beta\otimes\vec{\mathbf{e}}_k,\\ &\frac{\partial^2 I_2}{\partial \boldsymbol{F}^2} = 2\left(2F_{k\beta}F_{i\alpha} + I_1\delta_{ik}\delta_{\alpha\beta} - \delta_{ik}c_{\alpha\beta} - \delta_{\alpha\beta}b_{ik} - F_{i\beta}F_{k\alpha}\right)\vec{\mathbf{e}}_\alpha\otimes\vec{\mathbf{e}}_i\otimes\vec{\mathbf{e}}_\beta\otimes\vec{\mathbf{e}}_k,\\ &\frac{\partial^2 I_3}{\partial \boldsymbol{F}^2} = 2I_3\left(2F^{-1}_{\alpha i}F^{-1}_{\beta k} - F^{-1}_{\alpha k}F^{-1}_{\beta i}\right)\vec{\mathbf{e}}_\alpha\otimes\vec{\mathbf{e}}_i\otimes\vec{\mathbf{e}}_\beta\otimes\vec{\mathbf{e}}_k,\ \frac{\partial^2 I_5}{\partial \boldsymbol{F}^2} = 2D_{l\alpha}D_{l\beta}\delta_{ik}\vec{\mathbf{e}}_\alpha\otimes\vec{\mathbf{e}}_i\otimes\vec{\mathbf{e}}_\beta\otimes\vec{\mathbf{e}}_k,\\ &\frac{\partial^2 I_6}{\partial \boldsymbol{F}^2} = 2\begin{pmatrix}JF_{k\alpha}D_{l\beta}D_i + JF_{i\beta}D_{l\alpha}D_k + c_{\alpha\gamma}D_{l\gamma}D_{l\beta}\delta_{ik}\\ +c_{\beta\gamma}D_{l\gamma}D_{l\alpha}\delta_{ik} + J^2D_iD_k\delta_{\alpha\beta} + B_{ik}D_{l\alpha}D_{l\beta}\end{pmatrix}\vec{\mathbf{e}}_\alpha\otimes\vec{\mathbf{e}}_i\otimes\vec{\mathbf{e}}_\beta\otimes\vec{\mathbf{e}}_k,\end{aligned}\tag{A23}$$

$$\frac{\partial^2 I_5}{\partial \boldsymbol{F} \partial \boldsymbol{D}_l} = 2\left(JD_i\delta_{\alpha\beta} + D_{l\alpha}F_{i\beta}\right)\vec{\mathbf{e}}_\alpha \otimes \vec{\mathbf{e}}_i \otimes \vec{\mathbf{e}}_\beta,$$
$$\frac{\partial^2 I_6}{\partial \boldsymbol{F} \partial \boldsymbol{D}_l} = 2\left(Jc_{\alpha\beta}D_i + c_{\alpha\gamma}D_{l\gamma}F_{i\beta} + Jb_{im}D_m\delta_{\alpha\beta} + D_{l\alpha}b_{im}F_{m\beta}\right)\vec{\mathbf{e}}_\alpha \otimes \vec{\mathbf{e}}_i \otimes \vec{\mathbf{e}}_\beta, \tag{A24}$$

$$\frac{\partial^2 I_4}{\partial \boldsymbol{D}_l^2} = 2\delta_{\alpha\beta}\vec{\mathbf{e}}_\alpha \otimes \vec{\mathbf{e}}_\beta,\ \frac{\partial^2 I_5}{\partial \boldsymbol{D}_l^2} = 2c_{\alpha\beta}\vec{\mathbf{e}}_\alpha \otimes \vec{\mathbf{e}}_\beta,\ \frac{\partial^2 I_6}{\partial \boldsymbol{D}_l^2} = 2c_{\alpha\gamma}c_{\gamma\beta}\vec{\mathbf{e}}_\alpha \otimes \vec{\mathbf{e}}_\beta,\ (\alpha,\beta,\gamma = 1,2,3) \tag{A25}$$

where $c_{\alpha\beta}$, $c_{\alpha\gamma}$,..., F_{ia}, $F_{i\beta}$,..., $D_{l\alpha}$, $D_{l\beta}$,... are components of the right Cauchy-Green tensor, $\boldsymbol{c}$, deformation gradient, $\boldsymbol{F}$, the nominal electric displacement, $\boldsymbol{D}_1$, respectively, and $\vec{\mathbf{e}}_i$, $\vec{\mathbf{e}}_k$, $\vec{\mathbf{e}}_\alpha$, $\vec{\mathbf{e}}_\beta$ are the basis vectors.

In the following, we consider equi-biaxially stretched generalized ideal dielectrics (A3) with $\lambda_1 = \lambda_2 = \lambda$, such that Eqs. (A18-A20) reduce to more compact forms with the following nonzero components

$$\begin{aligned}
&\mathcal{A}_{01111} = \mathcal{A}_{02222} = 2\left[\Omega_1 + 2\lambda^2\Omega_{11} + \lambda^2\chi^2\left(\Omega_3 + 4\lambda^2\Omega_{13} + 2\lambda^4\chi^2\Omega_{33}\right)\right]/\chi,\\
&\mathcal{A}_{01122} = \mathcal{A}_{02211} = 4\left(\Omega_{11} + \chi^2\Omega_3 + 2\lambda^2\chi^2\Omega_{13} + \lambda^4\chi^4\Omega_{33}\right)\lambda^2/\chi,\\
&\mathcal{A}_{01133} = \mathcal{A}_{03311} = \mathcal{A}_{02233} = \mathcal{A}_{03322} = 4\left\{\chi\Omega_{11} + \lambda^2\chi\left[\Omega_3 + \left(\lambda^2 + \chi^2\right)\Omega_{13} + \lambda^4\chi^2\Omega_{33}\right]\right\} + 2D_3^2/\varepsilon,\\
&\mathcal{A}_{01212} = \mathcal{A}_{01313} = \mathcal{A}_{02121} = \mathcal{A}_{02323} = 2\Omega_1/\chi,\\
&\mathcal{A}_{01221} = \mathcal{A}_{02112} = \mathcal{A}_{01331} = \mathcal{A}_{02332} = \mathcal{A}_{03113} = \mathcal{A}_{03223} = -2\lambda^2\chi\Omega_3,\\
&\mathcal{A}_{03131} = \mathcal{A}_{03232} = 2\chi\Omega_1/\lambda^2 + D_3^2/\varepsilon,\\
&\mathcal{A}_{03333} = 2\left[\Omega_1 + 2\chi^2\Omega_{11} + \lambda^4\left(\Omega_3 + 4\chi^2\Omega_{13} + 2\lambda^4\chi^2\Omega_{33}\right)\right]\chi/\lambda^2 + 5D_3^2/\varepsilon,
\end{aligned} \tag{A26}$$

$$\Gamma_{0113} = \Gamma_{0223} = 2D_3/\varepsilon,\ \Gamma_{0131} = \Gamma_{0232} = \Gamma_{0311} = \Gamma_{0322} = D_3/\varepsilon,\ \Gamma_{0333} = 4D_3/\varepsilon, \tag{A27}$$

$$K_{011} = K_{022} = K_{033} = 1/\varepsilon. \tag{A28}$$

For convenience, we hereinafter use the following shorthand notations

$$\begin{aligned}
&\varepsilon_{11} = 1/K_{011} = \varepsilon,\ \varepsilon_{33} = 1/K_{033} = \varepsilon,\\
&e_{15} = -\varepsilon_{11}\Gamma_{0131} = -D_3,\ e_{31} = -\varepsilon_{33}\Gamma_{0113} = -2D_3,\ e_{33} = -\varepsilon_{33}\Gamma_{0333} = -4D_3,\\
&c_{11} = \mathcal{A}_{01111} + \Gamma_{0113}e_{31},\ c_{12} = \mathcal{A}_{01122} + \Gamma_{0113}e_{31},\ c_{13} = \mathcal{A}_{01133} + \Gamma_{0113}e_{33},\\
&c_{33} = \mathcal{A}_{03333} + \Gamma_{0333}e_{33},\ c_{58} = \mathcal{A}_{01331} + \Gamma_{0131}e_{15},\ c_{55} = \mathcal{A}_{01313} + \Gamma_{0131}e_{15},\\
&c_{88} = \mathcal{A}_{03131} + \Gamma_{0131}e_{15},\ c_{69} = \mathcal{A}_{01221},\ c_{66} = \mathcal{A}_{01212}.
\end{aligned} \tag{A29}$$

Appendix B. In-plane wrinkles under out-of-plane electrical stimulus

B.1. Two-dimensional (2D) wrinkles under a transverse electric field/displacement

We look for 2D solutions to the incremental equations such that $\boldsymbol{u} = \boldsymbol{u}(x_1, x_3)$ and $\dot{\varphi} = \dot{\varphi}(x_1, x_3)$, where we introduce the incremental potential $\dot{\varphi}$ via $\dot{\boldsymbol{E}}_{l0} = -\mathrm{grad}\dot{\varphi}$ such that $(A16)_3$ is satisfied automatically.

For the considered 2D motion, the incremental governing equations (A16) reduce to

$$\frac{\partial \dot{T}_{011}}{\partial x_1} + \frac{\partial \dot{T}_{031}}{\partial x_3} = 0,\ \frac{\partial \dot{T}_{013}}{\partial x_1} + \frac{\partial \dot{T}_{033}}{\partial x_3} = 0,\ \frac{\partial \dot{D}_{l01}}{\partial x_1} + \frac{\partial \dot{D}_{l03}}{\partial x_3} = 0, \tag{B1}$$

where

$$\begin{aligned}
&\dot{T}_{011} = c_{11}\frac{\partial u_1}{\partial x_1} + c_{13}\frac{\partial u_3}{\partial x_3} + e_{31}\frac{\partial \dot{\varphi}}{\partial x_3}, \quad \dot{T}_{031} = c_{88}\frac{\partial u_1}{\partial x_3} + c_{58}\frac{\partial u_3}{\partial x_1} + e_{15}\frac{\partial \dot{\varphi}}{\partial x_1},\\
&\dot{T}_{013} = c_{58}\frac{\partial u_1}{\partial x_3} + c_{55}\frac{\partial u_3}{\partial x_1} + e_{15}\frac{\partial \dot{\varphi}}{\partial x_1}, \quad \dot{T}_{033} = c_{13}\frac{\partial u_1}{\partial x_1} + c_{33}\frac{\partial u_3}{\partial x_3} + e_{33}\frac{\partial \dot{\varphi}}{\partial x_3},
\end{aligned} \tag{B2}$$

$$\dot{D}_{l01} = e_{15}\left(\frac{\partial u_1}{\partial x_3} + \frac{\partial u_3}{\partial x_1}\right) - \varepsilon_{11}\frac{\partial \dot{\varphi}}{\partial x_1},\ \dot{D}_{l03} = e_{31}\frac{\partial u_1}{\partial x_1} + e_{33}\frac{\partial u_3}{\partial x_3} - \varepsilon_{33}\frac{\partial \dot{\varphi}}{\partial x_3}. \tag{B3}$$

B.2. Stroh formulation

We assume that solutions are harmonic in the direction of x_1:

$$\left\{u_1, u_3, \dot{D}_{l03}, \dot{T}_{031}, \dot{T}_{033}, \dot{\varphi}\right\} = \mathrm{e}^{\mathrm{i}kx_1}\left\{k^{-1}U_1, k^{-1}U_3, \mathrm{i}\Delta, \mathrm{i}\Sigma_{31}, \mathrm{i}\Sigma_{33}, k^{-1}\Phi\right\}, \tag{B4}$$

where U_{i}, Σ_{3i} $(i=1,3)$, Δ and Φ are functions of kx_3 only, $k=2\pi/\mathcal{L}$ is the positive 'wavenumber' and $\mathcal{L}$ is the 'wavelength' of wrinkles. Here we introduce the so-called Stroh vector as $\boldsymbol{\eta}=[\ \boldsymbol{U}\quad \boldsymbol{S}\ ]^{\mathrm{T}}$, where $\boldsymbol{U}=[\ U_1\quad U_3\quad \Delta\ ]^{\mathrm{T}}$, $\boldsymbol{S}=[\ \Sigma_{31}\quad \Sigma_{33}\quad \Phi\ ]^{\mathrm{T}}$ are the generalized displacement and traction vectors.

Then the full problem can be rewritten in Stroh form

$$\boldsymbol{\eta}' = \mathrm{i}\boldsymbol{N}\boldsymbol{\eta}, \tag{B5}$$

where the prime denotes differentiation with respect to kx_3, and N is the Stroh matrix, which can be partitioned as

$$\boldsymbol{N} = \begin{bmatrix} \boldsymbol{N}_1 & \boldsymbol{N}_2 \\ \boldsymbol{N}_3 & \boldsymbol{N}_1^{\dagger} \end{bmatrix}, \tag{B6}$$

where † denotes the Hermitian operator.

For equi-biaxial stretched plates, we define the following shorthand notation,

$$\begin{aligned} &a_1 = c_{88}, a_2 = \mathcal{A}_{03333}, a_3 = \mathcal{A}_{01133}, a_4 = \mathcal{A}_{03131}\varepsilon_{11}, a_5 = \mathcal{A}_{01111}, \\ &b_1 = e_{15}, c_1 = \Gamma_{0333}, c_2 = \Gamma_{0113}, d_1 = \varepsilon_{33}^{-1} = K_{033}, \end{aligned} \tag{B7}$$

so that the partitions of the Stroh matrix, $\boldsymbol{N}_1$, $\boldsymbol{N}_2$, and $\boldsymbol{N}_3$ read in compact forms as

$$\begin{aligned} &\boldsymbol{N}_1 = \begin{bmatrix} 0 & \tau_{33}/a_1 - 1 & 0 \\ -a_3/a_2 & 0 & -c_1/a_2 \\ 0 & -b_1\tau_{33}/a_1 & 0 \end{bmatrix}, \boldsymbol{N}_2 = \begin{bmatrix} 1/a_1 & 0 & -b_1/a_1 \\ 0 & 1/a_2 & 0 \\ -b_1/a_1 & 0 & a_4/a_1 \end{bmatrix}, \\ &\boldsymbol{N}_3 = \begin{bmatrix} a_3^2/a_2 - a_5 & 0 & a_3c_1/a_2 - c_2 \\ 0 & \tau_{33}^2/a_1 - \tau_{33} - \tau_{11} & 0 \\ a_3c_1/a_2 - c_2 & 0 & c_1^2/a_2 - d_1 \end{bmatrix}. \end{aligned} \tag{B8}$$

In particular, for the present work, there is no electric field external to the material and out-of-plane mechanical traction, thus $\tau_{33} \equiv 0$.

Using the following dimensionless moduli,

$$\begin{aligned} &\bar{a}_1 = a_1/\mu, \bar{a}_2 = a_2/\mu, \bar{a}_3 = a_3/\mu, \bar{a}_4 = a_4/(\varepsilon\mu), \\ &\bar{a}_5 = a_5/\mu, \bar{\tau}_{33} = \tau_{33}/\mu, \bar{\tau}_{11} = \tau_{11}/\mu, \bar{b}_1 = b_1/\sqrt{\mu\varepsilon}, \\ &\bar{c}_1 = c_1\sqrt{\varepsilon/\mu}, \bar{c}_2 = c_2\sqrt{\varepsilon/\mu}, \bar{d}_1 = \varepsilon d_1, \end{aligned} \tag{B9}$$

and fields,

$$\bar{U}_i = U_i, \bar{\Sigma}_{3i} = \Sigma_{3i}/\mu, \bar{\Delta}=\Delta/\sqrt{\mu\varepsilon}, \bar{\Phi} = \Phi\sqrt{\varepsilon/\mu}, \tag{B10}$$

for $i=1,3$, where $\bar{X}$ denotes a nondimensional measure of X, we normalize Eq. (B5) as

$$\bar{\boldsymbol{\eta}}' = \mathrm{i}\bar{\boldsymbol{N}}\bar{\boldsymbol{\eta}} \tag{B11}$$

where

$$\begin{aligned} &\bar{\boldsymbol{\eta}} = \begin{bmatrix} \bar{U}_1 & \bar{U}_3 & \bar{\Delta} & \vdots & \bar{\Sigma}_{31} & \bar{\Sigma}_{33} & \bar{\Phi} \end{bmatrix}^{\mathrm{T}} = \begin{bmatrix} \bar{\boldsymbol{U}} \vdots \bar{\boldsymbol{S}} \end{bmatrix}^{\mathrm{T}}, \bar{\boldsymbol{N}} = \begin{bmatrix} \bar{\boldsymbol{N}}_1 & \bar{\boldsymbol{N}}_2 \\ \bar{\boldsymbol{N}}_3 & \bar{\boldsymbol{N}}_1^{\dagger} \end{bmatrix}, \\ &\bar{\boldsymbol{N}}_1 = \begin{bmatrix} 0 & -1 & 0 \\ -\bar{a}_3/\bar{a}_2 & 0 & -\bar{c}_1/\bar{a}_2 \\ 0 & 0 & 0 \end{bmatrix}, \bar{\boldsymbol{N}}_2 = \begin{bmatrix} 1/\bar{a}_1 & 0 & -\bar{b}_1/\bar{a}_1 \\ 0 & 1/\bar{a}_2 & 0 \\ -\bar{b}_1/\bar{a}_1 & 0 & \bar{a}_4/\bar{a}_1 \end{bmatrix}, \\ &\bar{\boldsymbol{N}}_3 = \begin{bmatrix} \bar{a}_3^2/\bar{a}_2 - \bar{a}_5 & 0 & \bar{c}_1\bar{a}_3/\bar{a}_2 - \bar{c}_2 \\ 0 & -\bar{\tau}_{11} & 0 \\ \bar{c}_1\bar{a}_3/\bar{a}_2 - \bar{c}_2 & 0 & \bar{c}_1^2/\bar{a}_2 - \bar{d}_1 \end{bmatrix}. \end{aligned} \tag{B12}$$

B.3. Solutions for free-standing plates by the extended surface impedance matrix method

As all entries of N are constant, we may expect the solution to Eq. (B5) reads

$$\bar{\boldsymbol{\eta}}(kx_3) = \bar{\boldsymbol{\eta}}^0\mathrm{e}^{\mathrm{i}skx_3}, \tag{B13}$$

which carries out an eigen-problem of the eigenvalues, s, and eigenvectors, $\bar{\boldsymbol{\eta}}^0$, of the Stroh matrix,

$$\left(\bar{\boldsymbol{N}} - s\boldsymbol{I}\right)\bar{\boldsymbol{\eta}}^0 = \boldsymbol{0}. \tag{B14}$$

For Eq. (B14) to yield non-trivial solutions, the determinant of the coefficients matrix must vanish, i.e., $\det(\bar{\boldsymbol{N}} - s\boldsymbol{I}) = 0$, which can be expanded and rearranged as

$$
\begin{aligned}
&\bar{a}_1^2\bar{a}_2 s^6 - \bar{a}_1\Big[\big(\bar{a}_3 - \bar{b}_1\bar{c}_1\big)^2 - \bar{a}_1(\bar{\tau}_{11} - 2\bar{a}_3) + \big(\bar{a}_4 - \bar{b}_1^2\big)c_1^2 \\
&+\bar{a}_2\big(2\bar{b}_1\bar{c}_2 - \bar{a}_4\bar{d}_1 - \bar{a}_5)\big)\Big]s^4 + \Big\{\bar{a}_5\big(\bar{a}_1 - \bar{b}_1\bar{c}_1\big)^2 \\
&-\bar{a}_3\big(\bar{a}_4 - \bar{b}_1^2\big)\big(\bar{a}_3\bar{d}_1 - 2\bar{c}_1\bar{c}_2\big) - \bar{a}_1\big(2\bar{b}_1\bar{c}_2 - \bar{a}_4\bar{d}_1 - \bar{a}_5\big)\bar{\tau}_{11} \\
&+\bar{a}_1\Big[\bar{a}_4\big(\bar{c}_1\bar{c}_2 - \bar{a}_3\bar{d}_1\big) + \bar{c}_2\big(\bar{a}_4\bar{c}_1 + \bar{a}_3\bar{b}_1\big) - \bar{a}_3\big(\bar{a}_4\bar{d}_1 - \bar{b}_1\bar{c}_2\big)\Big] - \bar{a}_4\bar{a}_5\bar{c}_1^2 \\
&+\bar{a}_2\big(\bar{a}_4 - \bar{b}_1^2\big)\big(\bar{a}_5\bar{d}_1 - \bar{c}_2^2\big)\Big\}s^2 + \big(\bar{a}_5\bar{d}_1 - \bar{c}_2^2\big)\Big[\bar{a}_1\bar{a}_4 + \big(\bar{a}_4 - \bar{b}_1^2\big)()\bar{\tau}_{11}\Big] = 0.
\end{aligned}
\tag{B15}
$$

This bicubic equation indicates in principle that there are six sets of eigenvectors $\bar{\boldsymbol{\eta}}^{(j)}$, $j = 1, 2, ..., 6$, of which the general expressions can be derived through linear manipulations of matrix as

$$
\bar{\boldsymbol{\eta}}^{(j)} = \begin{bmatrix}
s_j\left\{\dfrac{s_j^2\bar{b}_1}{\bar{a}_1} + \dfrac{(\bar{b}_1^2 - \bar{a}_4)(\bar{a}_3\bar{c}_1 - \bar{a}_2\bar{c}_2) - \bar{a}_1\big[\bar{b}_1(\bar{a}_3 - \bar{\tau}_{11}) + \bar{a}_4\bar{c}_1\big]}{\bar{a}_1^2\bar{a}_2}\right\} + \dfrac{\bar{a}_4\bar{c}_2}{s_j\bar{a}_1\bar{a}_2} - \dfrac{(\bar{b}_1^2 - \bar{a}_4)\bar{\tau}_{11}}{s_j\bar{a}_1^2\bar{a}_2/\bar{c}_2} \\
-\left[\dfrac{s_j^2(\bar{a}_3\bar{b}_1 - \bar{a}_4\bar{c}_1)}{\bar{a}_1\bar{a}_2} + \dfrac{(\bar{b}_1^2 - \bar{a}_4)(\bar{a}_5\bar{c}_1 - \bar{a}_3\bar{c}_2)}{\bar{a}_1^2\bar{a}_2} + \dfrac{\bar{a}_4\bar{c}_2 - \bar{a}_5\bar{b}_1}{\bar{a}_1\bar{a}_2}\right] \\
-\dfrac{\bar{a}_4}{\bar{a}_1}s_j^3 + s_j\left[\dfrac{(\bar{b}_1^2 - \bar{a}_4)(\bar{a}_2\bar{a}_5 - \bar{a}_3^2)}{\bar{a}_1^2\bar{a}_2} + \dfrac{a_4(2\bar{a}_3 - \bar{\tau}_{11})}{\bar{a}_1\bar{a}_2}\right] + \dfrac{1}{s_j}\left[\dfrac{(\bar{a}_1^2 - \bar{a}_4)\bar{a}_5\bar{\tau}_{11}}{\bar{a}_1^2\bar{a}_2} - \dfrac{\bar{a}_4\bar{a}_5}{\bar{a}_1\bar{a}_2}\right] \\
s_j^2\left[\dfrac{\bar{a}_4\bar{c}_2 - \bar{a}_5\bar{b}_1}{\bar{a}_1} + \dfrac{(\bar{a}_3\bar{b}_1 - \bar{a}_4\bar{c}_1)\bar{a}_3}{\bar{a}_1\bar{a}_2}\right] + \dfrac{\bar{a}_4(\bar{a}_5\bar{c}_1 - \bar{a}_3\bar{c}_2)}{\bar{a}_1\bar{a}_2} + \dfrac{(\bar{a}_4\bar{c}_2 - \bar{a}_5\bar{b}_1)\bar{\tau}_{11}}{\bar{a}_1\bar{a}_2} \\
-s_j\left[\dfrac{(\bar{a}_3\bar{b}_1 - \bar{a}_4\bar{c}_1)(\bar{a}_3 - \bar{\tau}_{11})}{\bar{a}_1\bar{a}_2} + \dfrac{\bar{a}_4\bar{c}_2 - \bar{a}_5\bar{b}_1}{\bar{a}_1}\right] + \dfrac{(\bar{a}_5\bar{c}_1 - \bar{a}_3\bar{c}_2)\big[(\bar{b}_1^2 - \bar{a}_4)\bar{\tau}_{11} - \bar{a}_1\bar{a}_4\big]}{s_j\bar{a}_1^2\bar{a}_2} \\
-s_j^4 - s_j^2\dfrac{\bar{a}_3(\bar{b}_1\bar{c}_1 - \bar{a}_3) + \bar{a}_2(\bar{a}_5 - \bar{b}_1\bar{c}_2) - \bar{a}_1(2\bar{a}_3 - \bar{\tau}_{11})}{\bar{a}_1\bar{a}_2} - \dfrac{\bar{c}_2(\bar{a}_3 - \bar{\tau}_{11})}{\bar{a}_1\bar{a}_2/\bar{b}_1} - \dfrac{\bar{a}_1 - \bar{b}_1\bar{c}_1 + \bar{\tau}_{11}}{\bar{a}_1\bar{a}_2/\bar{a}_5}
\end{bmatrix}.
\tag{B16}
$$

After calculating the eigenvalues s_j and eigenvectors $\bar{\boldsymbol{\eta}}^{(j)}$, $j = 1, 2, ..., 6$, we can construct the full solution to Eq. (B5) for an SEA plate as

$$
\bar{\boldsymbol{\eta}}(kx_3) = \begin{bmatrix} \bar{\boldsymbol{U}}(kx_3) \\ \bar{\boldsymbol{S}}(kx_3) \end{bmatrix} = \sum_{j=1}^{6} h_j \bar{\boldsymbol{\eta}}^{(j)} \mathrm{e}^{\mathrm{i}s_j kx_3},
\tag{B17}
$$

where h_j for $j = 1, 2, ..., 6$ are arbitrary constants to be determined from the boundary conditions.

For the considered energy functions, the eigenvalues come in conjugate pairs and are pure imaginary. So we may write them as $s_j = \mathrm{i}r_j$ and $s_{j+3} = -\mathrm{i}r_j$ for $j = 1, 2, 3$, where r_1, r_2, r_3 are real. Accordingly, the eigenvectors of conjugate pairs come as $\bar{\boldsymbol{\eta}}^{(j)} = \overline{\bar{\boldsymbol{\eta}}^{(j+3)}}$ for $j = 1, 2, 3$.

The above analysis will turn out to be the most efficient for the voltage-controlled SEA plates. While for the charge-controlled boundary value problem, the Stroh vector should be modified properly, by exchanging the third and sixth components of $\bar{\boldsymbol{\eta}}(kx_3)$. That is, the modified Stroh vector for the charge-controlled plates reads $\bar{\boldsymbol{\eta}}^*(kx_3) = [\ \bar{\boldsymbol{U}}^*(kx_3)\quad \bar{\boldsymbol{S}}^*(kx_3)\ ]^{\mathrm{T}}$, where $\bar{\boldsymbol{U}}^* = [\ \bar{U}_1\quad \bar{U}_3\quad \bar{\Phi}\ ]^{\mathrm{T}}$, $\bar{\boldsymbol{S}}^* = [\ \bar{\Sigma}_{31}\quad \bar{\Sigma}_{33}\quad \bar{\Delta}\ ]^{\mathrm{T}}$. In this paper, the variables for the charge-controlled problem are distinguished by a superscript of "*". Then the corresponding eigenvalues and eigenvectors can be easily obtained by following the standard procedure presented above.

The incremental equations are solved subject to the mechanical traction-free condition as well as the prescribed electric condition (either electric potential or charges) on the top and bottom faces of the plate, i.e.,

$$
(I) \qquad \bar{\boldsymbol{S}}(kh/2) = \bar{\boldsymbol{S}}(-kh/2) = \boldsymbol{0},
\tag{B18}
$$

$$
(II) \qquad \bar{\boldsymbol{S}}^*(kh/2) = \bar{\boldsymbol{S}}^*(-kh/2) = \boldsymbol{0},
\tag{B19}
$$

for the voltage- and charge-controlled scenarios, respectively.

Eqs. (B18) and (B19) can be expanded using Eq. (B17) as

$$
(I) \qquad \begin{bmatrix} \bar{\boldsymbol{S}}(kh/2) \\ \bar{\boldsymbol{S}}(-kh/2) \end{bmatrix} = \begin{bmatrix}
F_1E_1^- & F_2E_2^- & F_3E_3^- & F_4E_1^+ & F_5E_2^+ & F_6E_3^+ \\
G_1E_1^- & G_2E_2^- & G_3E_3^- & G_4E_1^+ & G_5E_2^+ & G_6E_3^+ \\
H_1E_1^- & H_2E_2^- & H_3E_3^- & H_4E_1^+ & H_5E_2^+ & H_6E_3^+ \\
F_1E_1^+ & F_2E_2^+ & F_3E_3^+ & F_4E_1^- & F_5E_2^- & F_6E_3^- \\
G_1E_1^+ & G_2E_2^+ & G_3E_3^+ & G_4E_1^- & G_5E_2^- & G_6E_3^- \\
H_1E_1^+ & H_2E_2^+ & H_3E_3^+ & H_4E_1^- & H_5E_2^- & H_6E_3^-
\end{bmatrix}
\begin{bmatrix} h_1 \\ h_2 \\ h_3 \\ h_4 \\ h_5 \\ h_6 \end{bmatrix} = \boldsymbol{0},
\tag{B20}
$$

$$(II)\qquad \begin{bmatrix}\bar{\boldsymbol{S}}^*(kh/2)\\ \bar{\boldsymbol{S}}^*(-kh/2)\end{bmatrix} = \begin{bmatrix} F_1E_1^- & F_2E_2^- & F_3E_3^- & F_4E_1^+ & F_5E_2^+ & F_6E_3^+ \\ G_1E_1^- & G_2E_2^- & G_3E_3^- & G_4E_1^+ & G_5E_2^+ & G_6E_3^+ \\ L_1E_1^- & L_2E_2^- & L_3E_3^- & L_4E_1^+ & L_5E_2^+ & L_6E_3^+ \\ F_1E_1^+ & F_2E_2^+ & F_3E_3^+ & F_4E_1^- & F_5E_2^- & F_6E_3^- \\ G_1E_1^+ & G_2E_2^+ & G_3E_3^+ & G_4E_1^- & G_5E_2^- & G_6E_3^- \\ L_1E_1^+ & L_2E_2^+ & L_3E_3^+ & L_4E_1^- & L_5E_2^- & L_6E_3^- \end{bmatrix} \begin{bmatrix} h_1\\ h_2\\ h_3\\ h_4\\ h_5\\ h_6\end{bmatrix} = \mathbf{0}, \tag{B21}$$

where $L_j = \bar{\eta}_3^{(j)}$, $F_j = \bar{\eta}_4^{(j)}$, $G_j = \bar{\eta}_5^{(j)}$, and $H_j = \bar{\eta}_6^{(j)}$ are the third to the sixth components of the eigenvector $\bar{\boldsymbol{\eta}}^{(j)}$, and $E_j^{\pm} = \mathrm{e}^{\pm r_j kh/2}$, for $j = 1, 2, ..., 6$. Since the eigenvalues are conjugate, we have $E_{j+3}^{\pm} = E_j^{\mp}$, for $j = 1, 2, 3$. For our choices of free energy densities, once giving $F_{j+3} = F_j$, it follows that $G_{j+3} = -G_j$, $H_{j+3} = H_j$, and $L_{j+3} = -L_j$, for $j = 1, 2, 3$. Then, two 3×3 blocks for the antisymmetric and symmetric modes can be decoupled from Eqs. (B20) and (B21) through some linear manipulations (Nayfeh, 1995), as

$$(I)\qquad \begin{vmatrix} F_1C_1 & F_2C_2 & F_3C_3\\ G_1S_1 & G_2S_2 & G_3S_3\\ H_1C_1 & H_2C_2 & H_3C_3 \end{vmatrix} \times \begin{vmatrix} F_1S_1 & F_2S_2 & F_3S_3\\ G_1C_1 & G_2C_2 & G_3C_3\\ H_1S_1 & H_2S_2 & H_3S_3 \end{vmatrix} = 0, \tag{B22}$$

$$(II)\qquad \begin{vmatrix} L_1S_1 & L_2S_2 & L_3S_3\\ F_1C_1 & F_2C_2 & F_3C_3\\ G_1S_1 & G_2S_2 & G_3S_3 \end{vmatrix} \times \begin{vmatrix} L_1C_1 & L_2C_2 & L_3C_3\\ F_1S_1 & F_2S_2 & F_3S_3\\ G_1C_1 & G_2C_2 & G_3C_3 \end{vmatrix} = 0, \tag{B23}$$

where $C_j = \cosh(r_j kh/2)$ and $S_j = \sinh(r_j kh/2)$. Here the antisymmetric mode is described by the left determinant and the symmetric mode by the right one. The expressions for the dispersions are thus deduced in general,

$$(\mathrm{I})\qquad \begin{aligned} &G_1(F_3H_2 - F_2H_3)\tanh(r_1kh/2)\\ &+ G_2(F_1H_3 - F_3H_1)\tanh(r_2kh/2)\\ &+ G_3(F_2H_1 - F_1H_2)\tanh(r_3kh/2) = 0, \end{aligned} \tag{B24}$$

$$(\mathrm{II})\qquad \begin{aligned} &F_1(G_2L_3 - G_3L_2)\coth(r_1kh/2)\\ &+ F_2(G_3L_1 - G_1L_3)\coth(r_2kh/2)\\ &+ F_3(G_1L_2 - G_2L_1)\coth(r_3kh/2) = 0, \end{aligned} \tag{B25}$$

for the antisymmetric mode and,

$$(\mathrm{I})\qquad \begin{aligned} &G_1(F_3H_2 - F_2H_3)\coth(r_1kh/2)\\ &+ G_2(F_1H_3 - F_3H_1)\coth(r_2kh/2)\\ &+ G_3(F_2H_1 - F_1H_2)\coth(r_3kh/2) = 0, \end{aligned} \tag{B26}$$

$$(\mathrm{II})\qquad \begin{aligned} &F_1(G_2L_3 - G_3L_2)\tanh(r_1kh/2)\\ &+ F_2(G_3L_1 - G_1L_3)\tanh(r_2kh/2)\\ &+ F_3(G_1L_2 - G_2L_1)\tanh(r_3kh/2) = 0, \end{aligned} \tag{B27}$$

for the symmetric mode. The kh is determined by the initial thickness of the plate and the wavelength of wrinkles: $kh = 2\pi\chi H/\mathcal{L}$, which are easy to measure in experiments.

B.4. Thin-plate/long-wave and thick-plate/short-wave instabilities

In this section, our insights are shed into two extreme cases: the thin-plate (long-wave) limit (TPL) as $H/\mathcal{L} \to 0$ and the thick-plate (short-wave) limit (SWL) as $H/\mathcal{L} \to \infty$.

First, we give the TPL using $\det[\bar{\boldsymbol{N}}_3] = 0$ and $\det[\bar{\boldsymbol{N}}_3^*] = 0$ (Shuvalov, 2000), which may factorize as follows

$$\left(\bar{\tau}_{33}^2/\bar{a}_1 - \bar{\tau}_{33} - \bar{\tau}_{11}\right)\left[\left(\bar{a}_3^2 - \bar{a}_2\bar{a}_5\right)\left(\bar{c}_1^2 - \bar{a}_2\bar{d}_1\right) - (\bar{a}_3\bar{c}_1 - \bar{a}_2\bar{c}_2)^2\right]\bar{a}_2^{-2} = 0, \tag{B28}$$

for the voltage-controlled plates and

$$\left(\bar{a}_3^2/\bar{a}_2 - \bar{a}_5\right)\left[\left(\bar{\tau}_{33}^2/\bar{a}_1 - \bar{\tau}_{33} - \bar{\tau}_{11}\right)\bar{a}_4/\bar{a}_1 - \left(\bar{\tau}_{33}\bar{b}_1/\bar{a}_1\right)^2\right] = 0, \tag{B29}$$

for the charged-controlled plates, respectively.

With the surface traction-free condition applied, the buckling condition of the symmetric mode reduces to

$$\left(\bar{a}_3^2 - \bar{a}_2\bar{a}_5\right)\left(\bar{c}_1^2 - \bar{a}_2\bar{d}_1\right) - (\bar{a}_3\bar{c}_1 - \bar{a}_2\bar{c}_2)^2 = 0, \tag{B30}$$

for the voltage-controlled plates and

$$\bar{a}_3^2/\bar{a}_2 - \bar{a}_5 = 0, \tag{B31}$$

for the charge-controlled plates, respectively. Note that Eq. (B31), i.e.,

$$\mathcal{A}_{01133}^2 = \mathcal{A}_{01111}\mathcal{A}_{03333}, \tag{B32}$$

is in general not true. It means that this case does not have non-trivial TPL, which is also supported by the numerical results as shown in Figs. C9–C11. Furthermore, independent of the electrical boundary conditions, the antisymmetric buckling condition is given as

$$\bar{\tau}_{11} = 0. \tag{B33}$$

Next, the SWL is found from the dispersion equations (B24 and B25) by replacing the terms of "tanh (*)/coth (*)" with 1 as $H/\mathcal{L} \to \infty$. They read

$$G_1(F_3H_2 - F_2H_3) + G_2(F_1H_3 - F_3H_1) + G_3(F_2H_1 - F_1H_2) = 0, \tag{B34}$$

for the voltage-controlled plates and

$$F_1(G_2L_3 - G_3L_2) + F_2(G_3L_1 - G_1L_3) + F_3(G_1L_2 - G_2L_1) = 0, \tag{B35}$$

for the charge-controlled plates, respectively.

B.5. Explicit expressions of eigenvalues and eigenvectors for special energy densities

One key point of our method is to obtain the eigenvector so that the decoupled dispersion equations can be solved in an explicit way, of which the difficulty mainly comes from solving the characteristic Eq. (B15). Obviously, it is quite cumbersome to get analytical roots from such a tedious bicubic equation in the most general sense. Consider the ideal SEA materials (A3) with the constraint: $\partial^2\bar{W}/\partial I_1\partial I_3 \triangleq \bar{W}_{13} = 0$, for which Eq. (B15) can be written as

$$(s^2+1)\left[n_0 s^4 - (n_0 - n_1)s^2 + n_3\right] = 0, \tag{B36}$$

where

$$\begin{aligned}
n_0 &= \chi^2\overline{W}_1\left[-\overline{D}_3^2 J^{-1} + 2\chi^2\left(\lambda^{-4}\overline{W}_{11} + \lambda^4\overline{\Omega}_{33}\right)\right],\\
n_0 - n_1 &= \left(\overline{D}_3^2 J^{-1} - 2J^2\overline{\Omega}_{33}\right)\left[\left(\lambda^2+\chi^2\right)\overline{W}_1 + 2\left(\lambda^2-\chi^2\right)^2\overline{W}_{11}\right]\\
&\quad - \lambda^{-4}\overline{W}_1\left[\left(\lambda^2-\chi^2\right)\overline{W}_1 + 2\chi^2\left(3\lambda^2-\chi^2\right)\overline{W}_{11}\right],\\
n_3 &= \overline{W}_1\left[\left(\chi^{-2}-\lambda^{-2}\right)\overline{W}_1 + 2\lambda^2\left(\chi^{-2}\overline{W}_{11} + J^2\Omega_{33}\right) - \overline{D}_3^2\chi^{-1}\right].
\end{aligned} \tag{B37}$$

Here we have $\overline{\Omega} = \Omega/\mu$, $\partial^2\overline{W}/\partial I_1^2 \triangleq \overline{W}_{11}$ and the six eigenvalues are solved as

$$\begin{aligned}
s_1 &= \mathrm{i}, \qquad s_4 = -s_1 = -\mathrm{i},\\
s_{2,3} &= \mathrm{i}\sqrt{\frac{\begin{array}{c}\left(\overline{D}_3^2 - 2J^3\overline{\Omega}_{33}\right)\left[\left(\lambda^2+\chi^2\right) + 2\left(\lambda^2-\chi^2\right)^2\overline{W}_{11}/\overline{W}_1\right]\\ -\lambda^{-2}\chi\overline{W}_1\left[\left(\lambda^2-\chi^2\right) + 2\chi^2\left(3\lambda^2-\chi^2\right)\overline{W}_{11}/\overline{W}_1\right]\end{array}}{2\chi^2\left[\overline{D}_3^2 - 2J\chi^2\left(\lambda^{-4}\overline{W}_{11} + \lambda^4\overline{\Omega}_{33}\right)\right]} \pm \frac{(\lambda+\chi)|\lambda-\chi|\sqrt{\begin{array}{l}\left\{\left(\overline{D}_3^2 - 2J^3\overline{\Omega}_{33}\right)\left[1+2(\lambda-\chi)^2\overline{W}_{11}/\overline{W}_1\right]\right.\\ \left.+\lambda^{-2}\chi\overline{W}_1\left[1+2\chi(-2\lambda+\chi)\overline{W}_{11}/\overline{W}_1\right]\right\}\\ \left\{\left(\overline{D}_3^2 - 2J^3\overline{\Omega}_{33}\right)\left[1+2(\lambda+\chi)^2\overline{W}_{11}/\overline{W}_1\right]\right.\\ \left.+\lambda^{-2}\chi\overline{W}_1\left[1+2\chi(2\lambda+\chi)\overline{W}_{11}/\overline{W}_1\right]\right\}\end{array}}}{2\chi^2\left[\overline{D}_3^2 - 2J\chi^2\left(\lambda^{-4}\overline{W}_{11} + \lambda^4\overline{\Omega}_{33}\right)\right]}}\\
s_5 &= -s_2, \qquad s_6 = -s_3.
\end{aligned} \tag{B38}$$

In particular, for a generalized neo-Hookean ideal dielectric, we have $\bar{W}_{11}=0$. Thus Eq. (B38) reduces to

$$
\begin{aligned}
&s_1=\mathrm{i}, \qquad s_4=-s_1=-\mathrm{i},\\
&s_{2,3}=\mathrm{i}\sqrt{\begin{aligned}&\frac{\left(\overline{D}_3^2-2J^3\overline{\Omega}_{33}\right)\left(\lambda^2+\chi^2\right)-\lambda^{-2}\chi\left(\lambda^2-\chi^2\right)\overline{W}_1}{2\chi^2\left[\overline{D}_3^2-2J\chi^2\left(\lambda^4\overline{\Omega}_{33}\right)\right]}\\ &\pm\frac{(\lambda+\chi)|\lambda-\chi|\left|\overline{D}_3^2-2J^3\overline{\Omega}_{33}+\lambda^{-2}\chi\overline{W}_1\right|}{2\chi^2\left[\overline{D}_3^2-2J\chi^2\left(\lambda^4\overline{\Omega}_{33}\right)\right]}\end{aligned}},\\
&s_5=-s_2, \qquad s_6=-s_3.
\end{aligned}
\tag{B39}
$$

or

$$
\begin{aligned}
&s_1=\mathrm{i}, s_4=-s_1=-\mathrm{i},\\
&s_{2,3}=\mathrm{i}\left\{\frac{\lambda}{\chi},\sqrt{1-\frac{(\chi^{-1}-\lambda^{-2}\chi)\bar{W}_1}{\bar{D}_3^2-2J\chi^2(\lambda^4\bar{\Omega}_{33})}}\right\},\\
&s_5=-s_2, s_6=-s_3.
\end{aligned}
\tag{B40}
$$

The associated eigenvectors can be obtained by substitution of Eq. (B40) into Eq. (B16) as

$$
\begin{aligned}
&\bar{\boldsymbol{\eta}}^{(1)}=\begin{bmatrix}0\\0\\\mathrm{i}\\\bar{D}_3\\\mathrm{i}\bar{D}_3\\-1\end{bmatrix}_{s_1=\mathrm{i}},\ \bar{\boldsymbol{\eta}}^{(2)}=\begin{bmatrix}-\mathrm{i}\\\dfrac{\chi}{\lambda}\\-\mathrm{i}\bar{D}_3\\\bar{D}_3^2\lambda^{-1}\chi+2(\lambda^{-1}+\lambda^{-3}\chi^2)\bar{W}_1\\4\mathrm{i}\lambda^{-2}\chi\bar{W}_1\\-\bar{D}_3\lambda^{-1}\chi\end{bmatrix}_{s_2=\mathrm{i}\frac{\lambda}{\chi}},\\
&\bar{\boldsymbol{\eta}}^{(3)}=\begin{bmatrix}-\mathrm{i}\\\sqrt{1-\dfrac{(\chi^{-1}-\lambda^{-2}\chi)\bar{W}_1}{\bar{D}_3^2-2J\chi^2(\lambda^4\bar{\Omega}_{33})}}\\-\mathrm{i}\bar{D}_3\\\left(\bar{D}_3^2+4\lambda^{-2}\chi\bar{W}_1\right)\sqrt{1-\dfrac{(\chi^{-1}-\lambda^{-2}\chi)\bar{W}_1}{\bar{D}_3^2-2J\chi^2(\lambda^4\bar{\Omega}_{33})}}\\2\mathrm{i}(\chi^{-1}+\lambda^{-2}\chi)\bar{W}_1\\-\bar{D}_3\sqrt{1-\dfrac{(\chi^{-1}-\lambda^{-2}\chi)\bar{W}_1}{\bar{D}_3^2-2J\chi^2(\lambda^4\bar{\Omega}_{33})}}\end{bmatrix}_{s_3=\mathrm{i}\sqrt{1-\frac{(\chi^{-1}-\lambda^{-2}\chi)/2}{\bar{D}_3^2-2J\chi^2(\lambda^4\bar{\Omega}_{33})}}},\\
&\bar{\boldsymbol{\eta}}^{(4)}=\overline{\bar{\boldsymbol{\eta}}^{(1)}}, \bar{\boldsymbol{\eta}}^{(5)}=\overline{\bar{\boldsymbol{\eta}}^{(2)}}, \bar{\boldsymbol{\eta}}^{(6)}=\overline{\bar{\boldsymbol{\eta}}^{(3)}}.
\end{aligned}
\tag{B41}
$$

All these results reduce to that of the incompressible problem (Su et al., 2018b) once making $\chi=\lambda^{-2}$, $J=1$ and $\lim_{\nu\to 0.5}\overline{\Omega}_{33}=\infty$.

Appendix C. Complementary figures

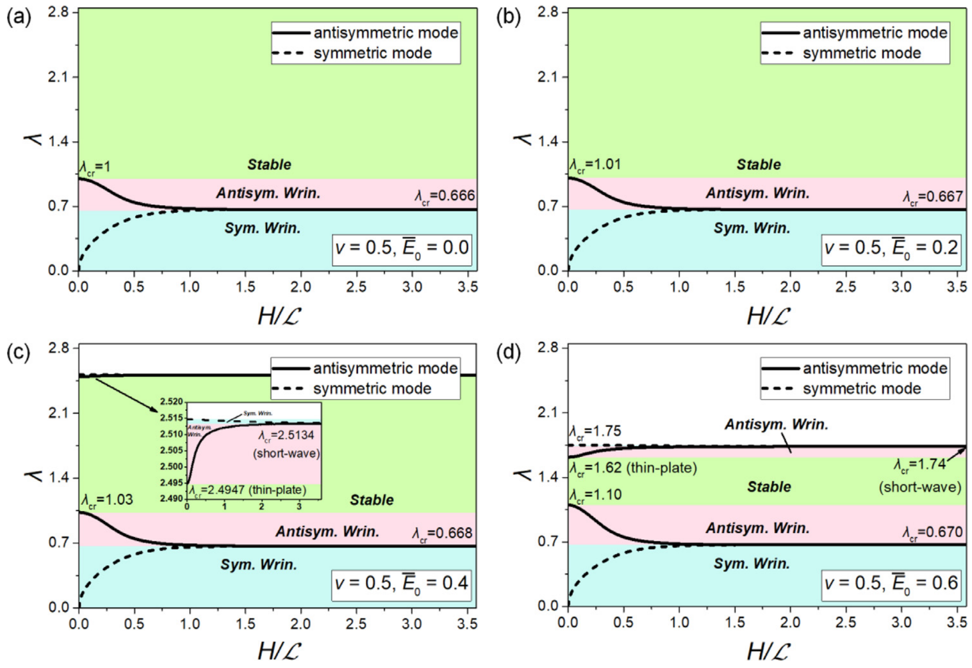

Fig. C1. Phase diagrams of wrinkling instability for equi-biaxially stretched incompressible neo-Hookean ideal SEA plates subject to sequential bias voltages ($\bar{E}_0$ =0.0, 0.2, 0.4, 0.6), where the solid and dashed lines correspond to the antisymmetric and symmetric wrinkles, respectively.

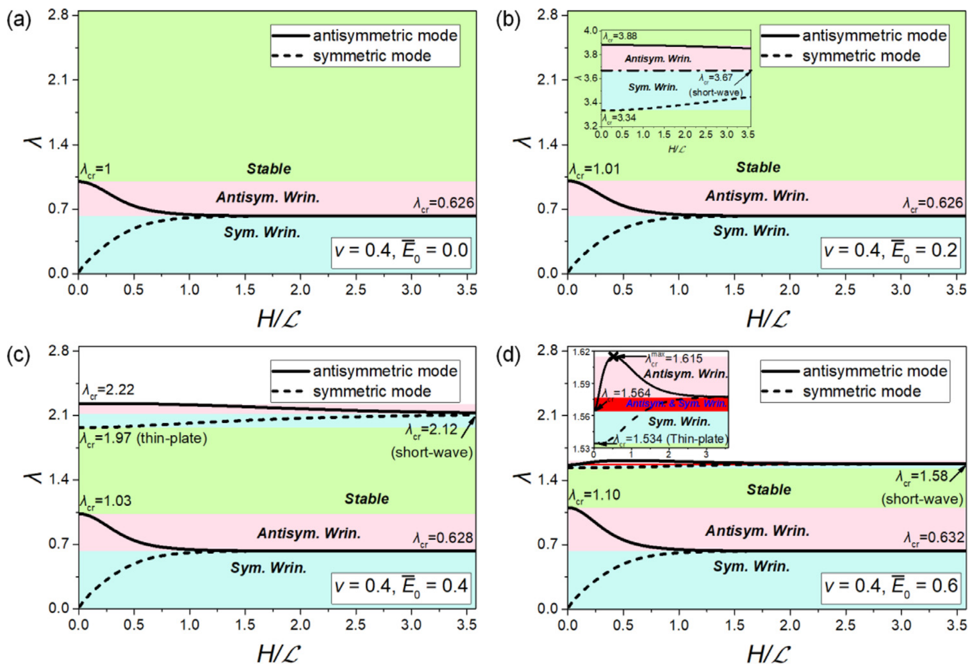

Fig. C2. Phase diagrams of wrinkling instability for equi-biaxially stretched slightly compressible neo-Hookean ideal SEA plates subject to sequential bias voltages ($\bar{E}_0$ =0.0, 0.2, 0.4, 0.6), where the solid and dashed lines correspond to the antisymmetric and symmetric wrinkles, respectively.

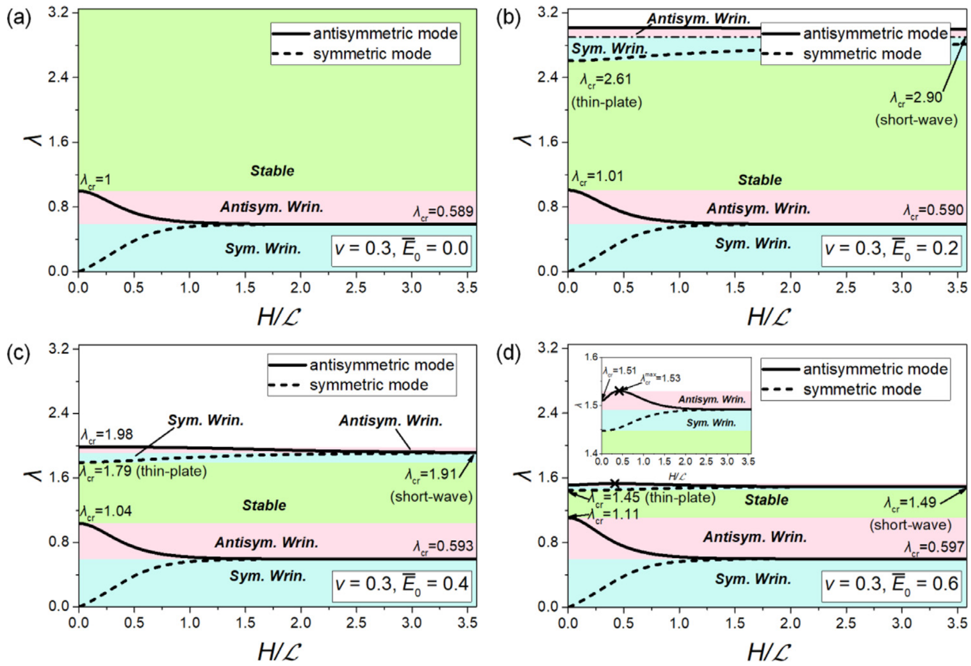

Fig. C3. Phase diagrams of wrinkling instability for equi-biaxially stretched moderately compressible neo-Hookean ideal SEA plates subject to sequential bias voltages ($\bar{E}_0$ =0.0, 0.2, 0.4, 0.6), where the solid and dashed lines correspond to the antisymmetric and symmetric wrinkles, respectively.

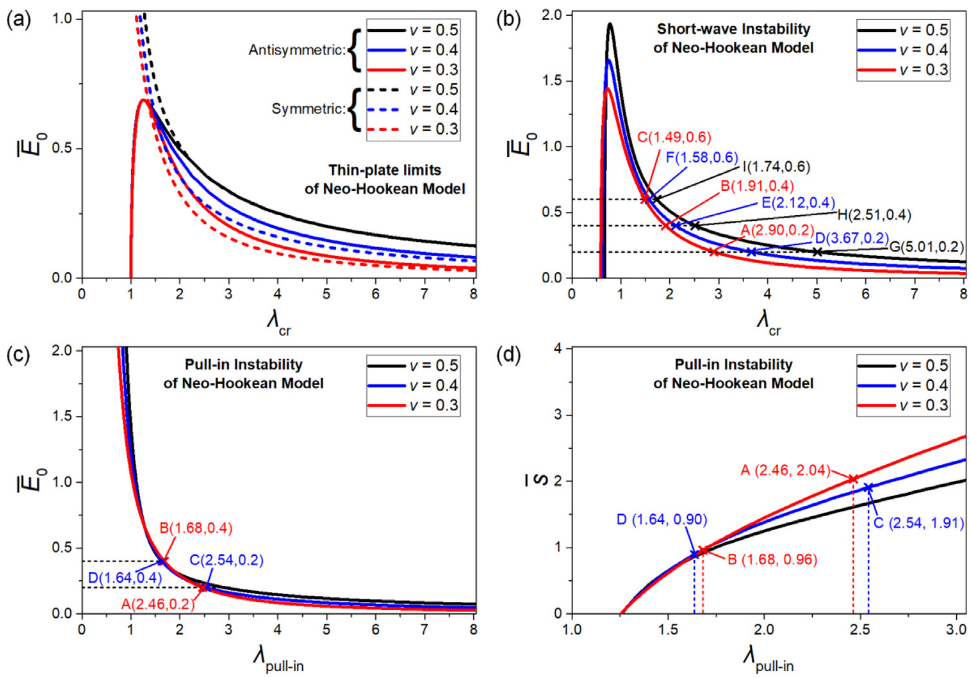

Fig. C4. Thin-plate limits, short-wave instability, and pull-in instability of equi-biaxially stretched neo-Hookean ideal SEA plates of different compressibility (ν =0.5, 0.4, 0.3).

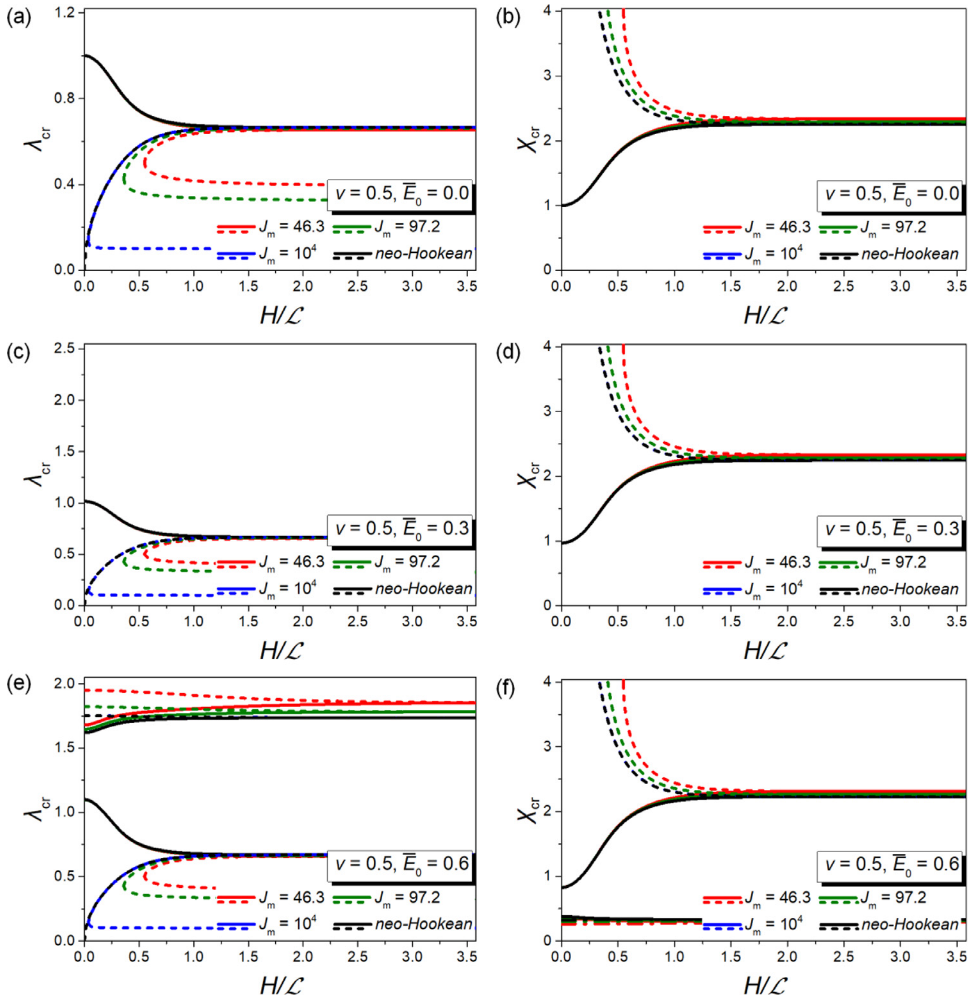

Fig. C5. Dispersion curves for equi-biaxially stretched incompressible ideal SEA plates of different chain extension limit (J_m =46.3, 97.2, 10^4, and infinity/neo-Hookean) subject to sequential constant bias voltages ($\bar{E}_0$ =0.0, 0.3, 0.6), where the solid and dashed lines correspond to the antisymmetric and symmetric wrinkles, respectively.

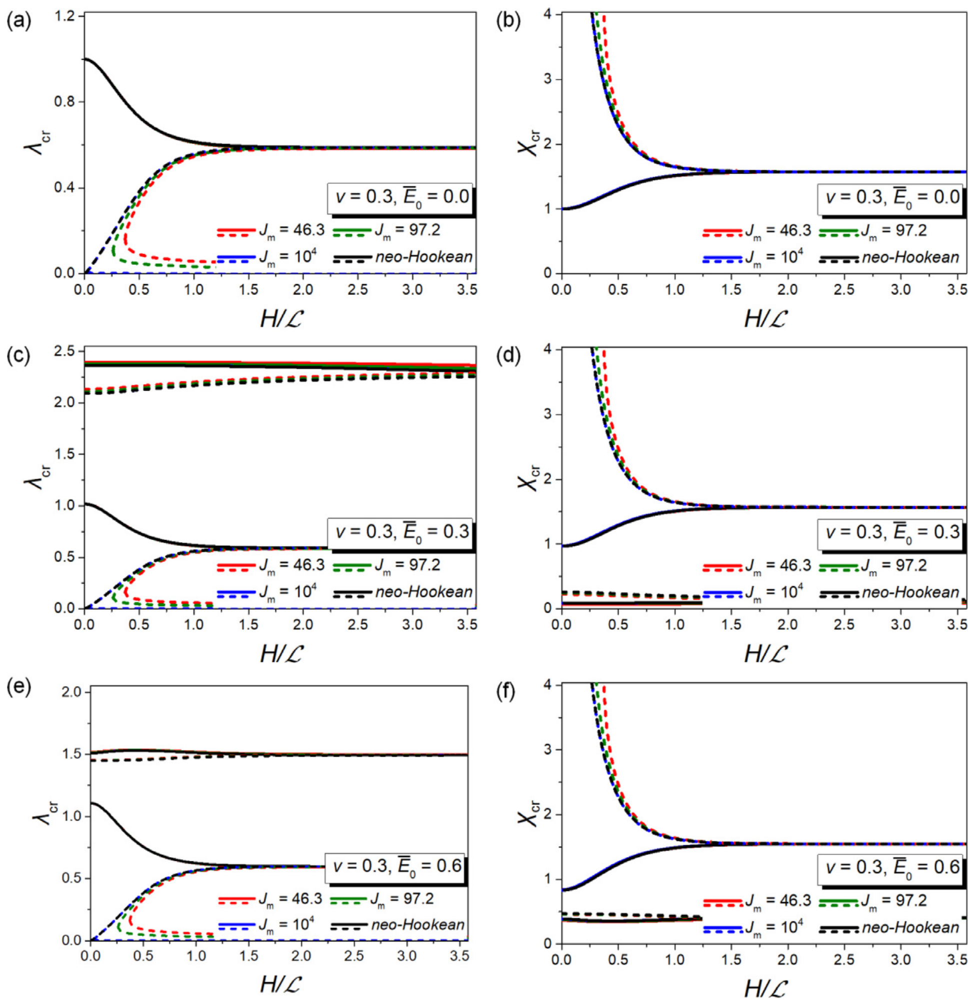

Fig. C6. Dispersion curves for equi-biaxially stretched moderately compressible ideal SEA plates of different chain extension limit (J_m =46.3, 97.2, 10^4, and infinity/neo-Hookean) subject to sequential constant bias voltages ($\bar{E}_0$ =0.0, 0.3, 0.6), where the solid and dashed lines correspond to the antisymmetric and symmetric wrinkles, respectively.

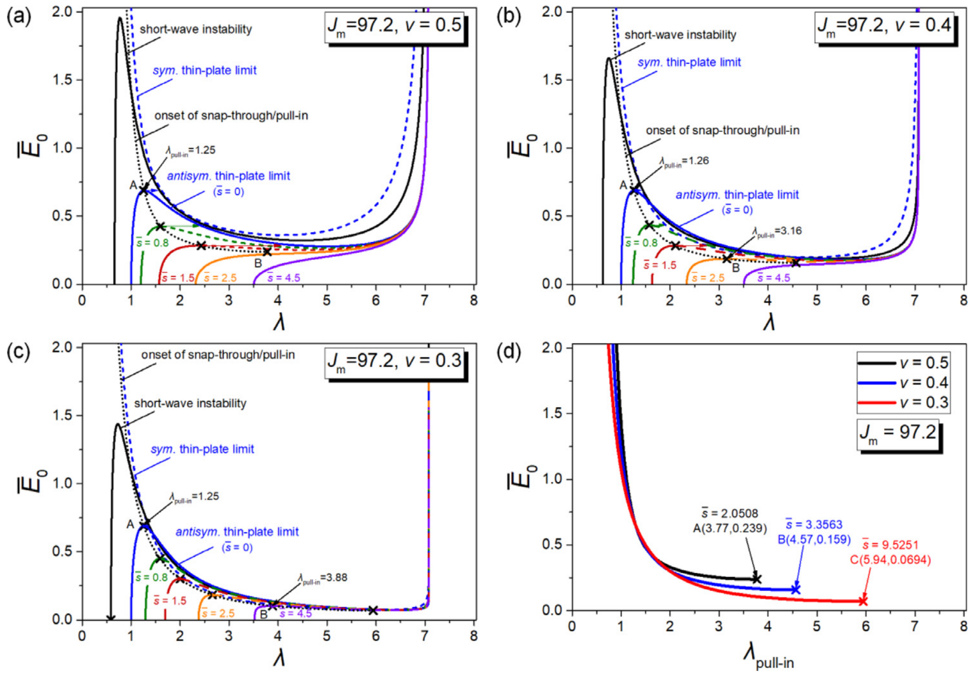

Fig. C7. Thin-plate and short-wave limits along with loading curves of various pre-stresses ($\bar{s}$ =0, 0.8, 1.5, 2.5 and 4.5) and critical curves for onset of pull-in for equi-biaxially stretched and voltage-controlled Gent (J_m = 97.2) ideal SEA plates with three kinds of compressibility (ν =0.5, 0.4, 0.3).

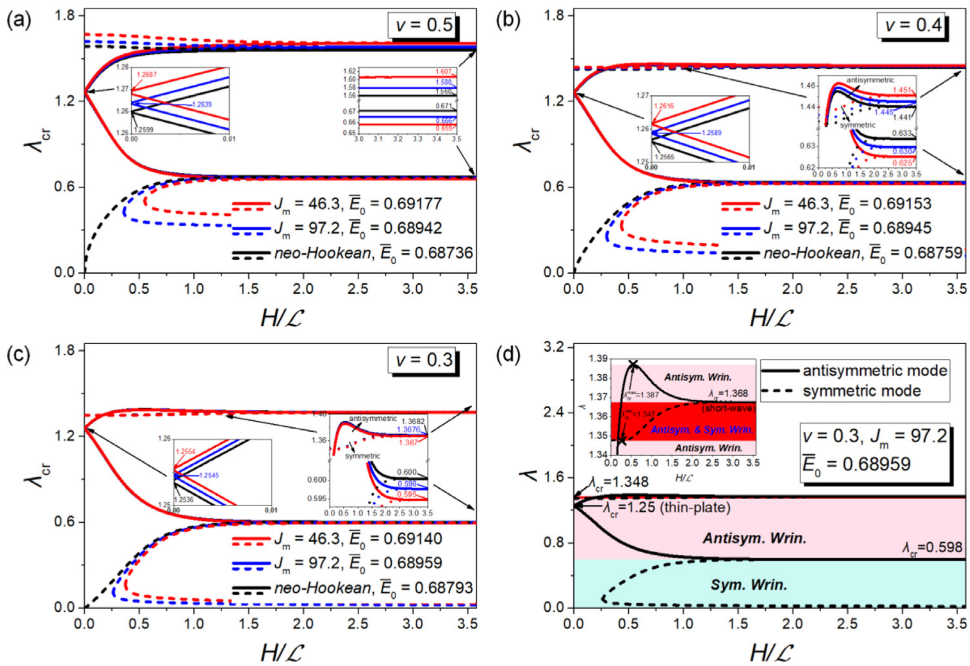

Fig. C8. Dispersion curves for ideal SEA plates of different chain extension limit (J_m =46.3, 97.2, and infinity/neo-Hookean) subject to equi-biaxial stretches and a constant voltage: (a) $\nu = 0.5$; (b) $\nu = 0.4$; (c) $\nu = 0.3$; (d) distribution of the stable and wrinkled regions for a Gent ideal SEA plate ($\nu = 0.3$, J_m =97.2) at $\bar{E}_0 = 0.68959$.

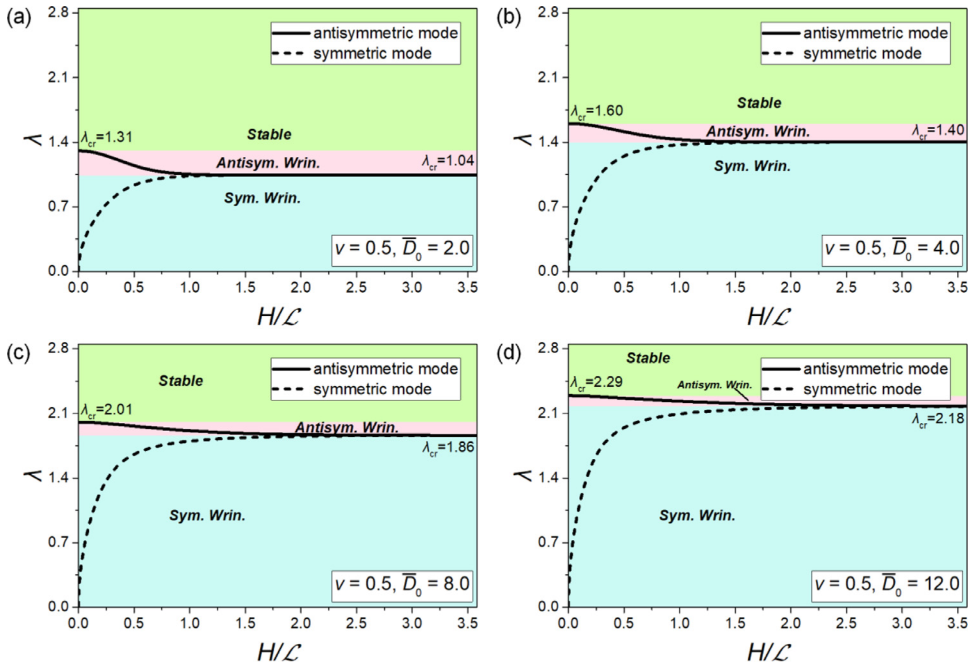

Fig. C9. Phase diagrams of wrinkling instability for equi-biaxially stretched incompressible neo-Hookean ideal SEA plates subject to sequential electrical charges on both sides ($\bar{D}_0$ =2.0, 4.0, 8.0, 12.0), where the solid lines and the dashed lines correspond to the antisymmetric wrinkles and the symmetric wrinkles, respectively. Note that the case of $\bar{D}_0 = 0$ may be identically referred to Figs. C.1 (a) for $\bar{E}_0 = 0$.

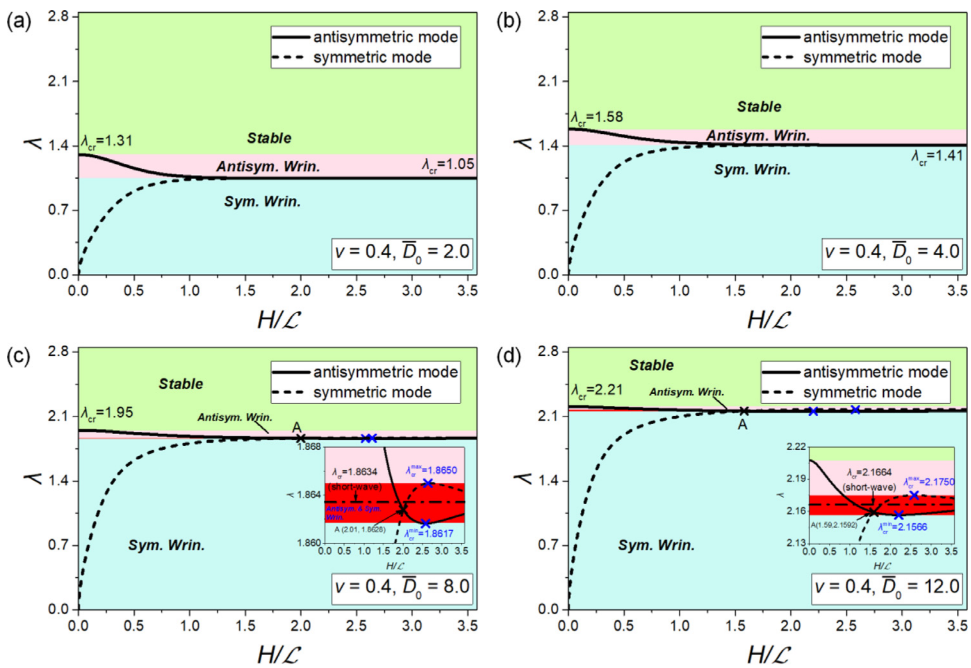

Fig. C10. Phase diagrams of wrinkling instability for equi-biaxially stretched slightly compressible neo-Hookean ideal SEA plates subject to sequential electrical charges on both sides ($\bar{D}_0$ =2.0, 4.0, 8.0, 12.0), where the solid lines and the dashed lines correspond to the antisymmetric wrinkles and the symmetric wrinkles, respectively. Note that the case of $\bar{D}_0 = 0$ may be identically referred to Figs. C.2 (a) for $\bar{E}_0 = 0$.

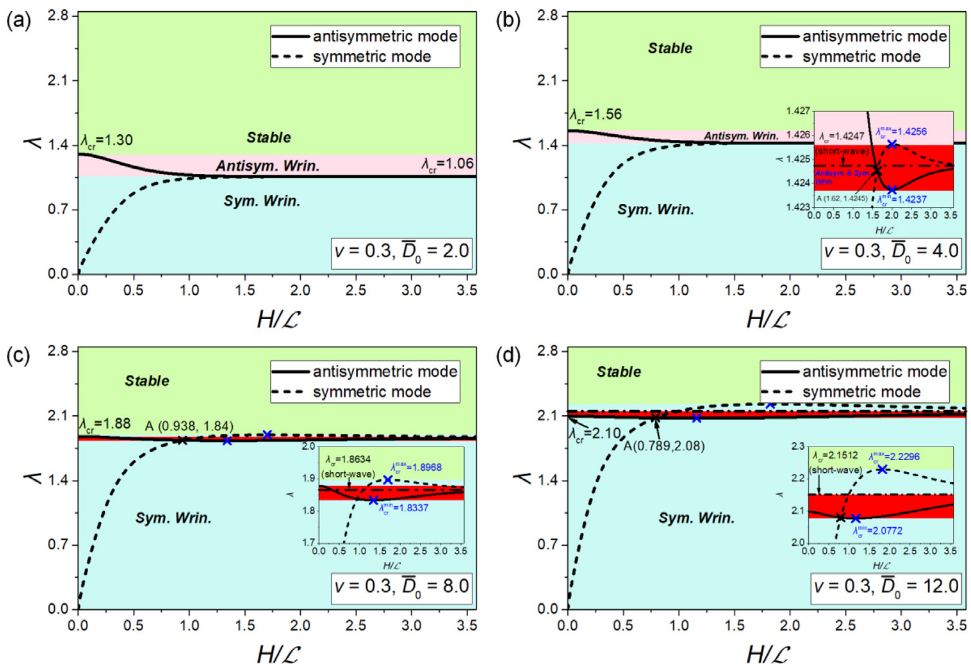

Fig. C11. Phase diagrams of wrinkling instability for equi-biaxially stretched moderately compressible neo-Hookean ideal SEA plates subject to sequential electrical charges on both sides ($\bar{D}_0$ =2.0, 4.0, 8.0, 12.0), where the solid lines and the dashed lines correspond to the antisymmetric and symmetric wrinkles, respectively. Note that the case of $\bar{D}_0 = 0$ may be identically referred to Figs. C.3 (a) for $\bar{E}_0 = 0$.

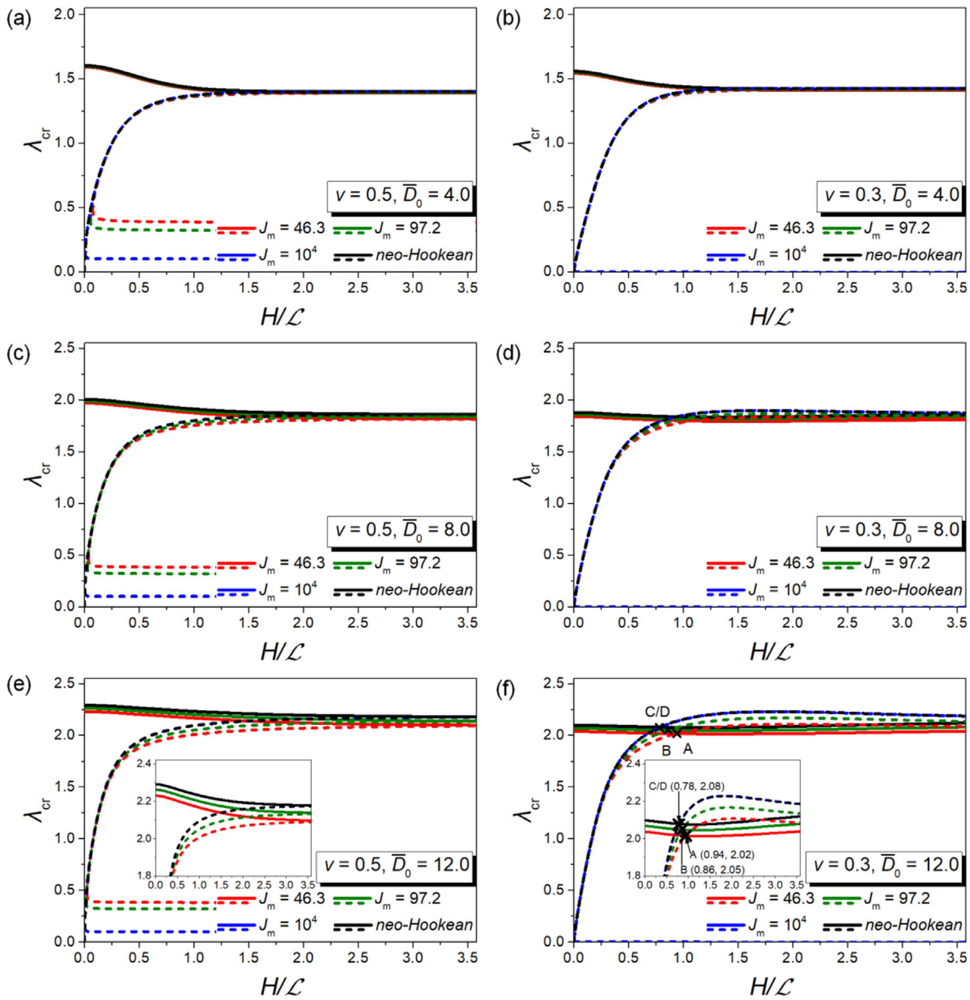

Fig. C12. Dispersion curves for equi-biaxially stretched incompressible and moderately compressible ideal SEA plates of different chain extension limit (J_m =46.3, 97.2, 10^4, and infinity/neo-Hookean) subject to constant charges sprayed on main faces ($\bar{D}_0$ =4.0, 8.0, 12.0).

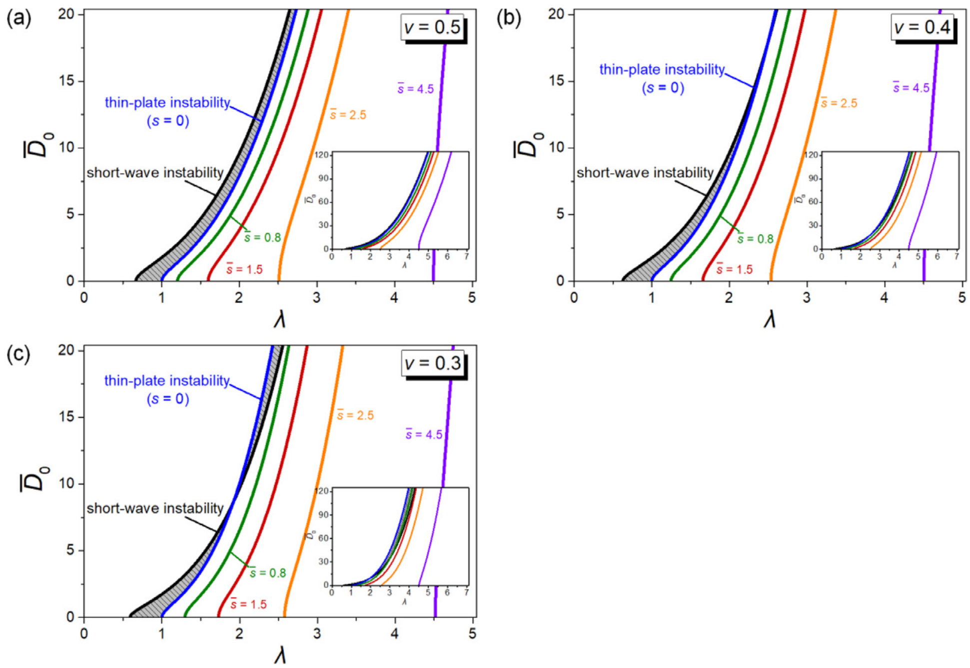

Fig. C13. Thin-plate and short-wave limits along with loading curves at various pre-stresses ($\bar{s}$ =0, 0.8, 1.5, 2.5 and 4.5) for equi-biaxially stretched and charge-controlled neo-Hookean ideal SEA plates with three types of compressibility (ν = 0.5, 0.4, 0.3).

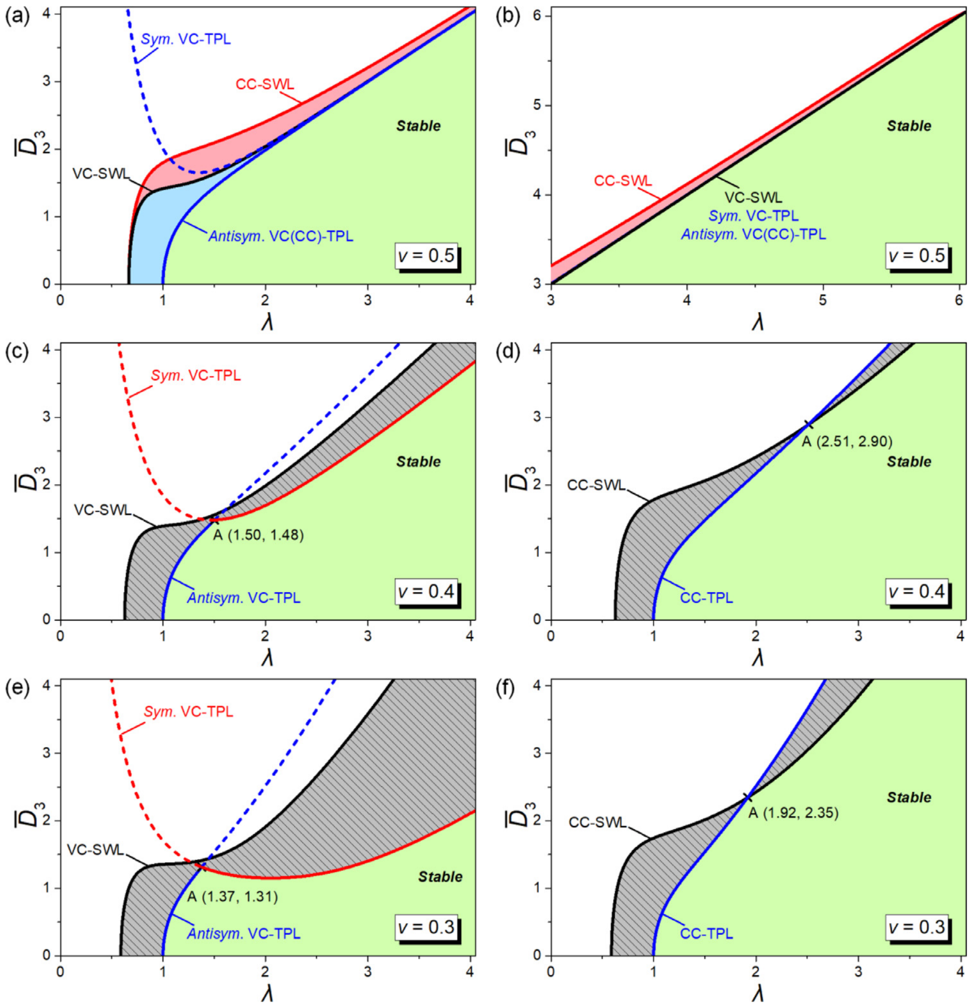

Fig. C14. Comparison of wrinkling instability between equi-biaxially stretched voltage- and charge-controlled neo-Hookean ideal SEA plates: true electric displacement, $\bar{D}_3$, versus stretch, λ. Here the "VC" and "CC" are abbreviations for voltage- and charge-controlled cases, respectively.

References

Acome, E., Mitchell, S., Morrissey, T., Emmett, M., Benjamin, C., King, M., et al. (2018). Hydraulically amplified self-healing electrostatic actuators with muscle-like performance. *Science, 359*(6371), 61–65.

An, L., Wang, F. F., Cheng, S. B., Lu, T. Q., & Wang, T. J. (2015). Experimental investigation of the electromechanical phase transition in a dielectric elastomer tube. *Smart Materials and Structures, 24*(3), Article 035006.

Bauer, S., Bauer-Gogonea, S., Graz, I., Kaltenbrunner, M., Keplinger, C., & Schwödiauer, R. (2014). 25th anniversary article: a soft future: from robots and sensor skin to energy harvesters. *Advanced Materials, 26*(1), 149–162.

Bertoldi, K., & Gei, M. (2011). Instabilities in multilayered soft dielectrics. *Journal of the Mechanics and Physics of Solids, 59*(1), 18–42.

Blok, J., & LeGrand, D. G. (1969). Dielectric breakdown of polymer films. *Journal of Applied Physics, 40*(1), 288–293.

Bortot, E., & Shmuel, G. (2018). Prismatic bifurcations of soft dielectric tubes. *International Journal of Engineering Science, 124*, 104–114.

Bortot, E., Springhetti, R., & Gei, M. (2015). Optimization of load-driven soft dielectric elastomer generators. *Procedia IUTAM, 12*, 42–51.

Boyce, M. C., & Arruda, E. M. (2000). Constitutive models of rubber elasticity: A review. *Rubber Chemistry and Technology, 73*(3), 504–523.

Burgess, I. W., & Levinson, M. (1972). The instability of slightly compressible rectangular rubberlike solids under biaxial loadings. *International Journal of Solids and Structures, 8*(2), 133–148.

Carrara, A., Maccaferri, N., Cerea, A., Bozzola, A., De Angelis, F., Proietti Zaccaria, R., et al. (2020). Plasmon hybridization in compressible metal-insulator-metal nanocavities: an optical approach for sensing deep sub-wavelength deformation. *Advanced Optical Materials, 8*(18), Article 2000609.

Cheng, L., & Feng, J. (2020). Facile fabrication of stretchable and compressible strain sensors by coating and integrating low-cost melamine foam scaffolds with reduced graphene oxide and poly (styrene-b-ethylene-butylene-b-styrene). *Chemical Engineering Journal, 398*, Article 125429.

Colonnelli, S., Saccomandi, G., & Zurlo, G. (2015). The role of material behavior in the performances of electroactive polymer energy harvesters. *Journal of Polymer Science Part B: Polymer Physics, 53*(18), 1303–1314.

Conroy Broderick, H., Righi, M., Destrade, M., & Ogden, R. W. (2020). Stability analysis of charge-controlled soft dielectric plates. *International Journal of Engineering Science, 151*, Article 103280.

De Tommasi, D., Puglisi, G., Saccomandi, G., & Zurlo, G. (2010). Pull-in and wrinkling instabilities of electroactive dielectric actuators. *Journal of Physics D: Applied Physics, 43*(32), Article 325501.

Destrade, M. (2015). Incremental equations for soft fibrous materials. In *Nonlinear Mechanics of Soft Fibrous Materials* (pp. 233–267). Vienna: Springer.

Destrade, M., Martin, P. A., & Ting, T. C. T. (2002). The incompressible limit in linear anisotropic elasticity, with applications to surface waves and elastostatics. *Journal of the Mechanics and Physics of Solids, 50*(7), 1453–1468.

Destrade, M., & Saccomandi, G. (2005). On finite amplitude elastic waves propagating in compressible solids. *Physical Review E, 72*(1), Article 016620.

Díaz-Calleja, R., Llovera-Segovia, P., Dominguez, J. J., Rosique, M. C., & Lopez, A. Q. (2013). Theoretical modelling and experimental results of electromechanical actuation of an elastomer. *Journal of Physics D: Applied Physics, 46*(23), Article 235305.

Díaz-Calleja, R., Llovera-Segovia, P., & Quijano-López, A. (2017). Complex bifurcation maps in electroelastic elastomeric plates. *International Journal of Solids and Structures, 113*, 70–84.

Dorfmann, A., & Ogden, R. W. (2010a). Nonlinear electroelastostatics: Incremental equations and stability. *International Journal of Engineering Science, 48*(1), 1–14.

Dorfmann, A., & Ogden, R. W. (2010b). Electroelastic waves in a finitely deformed electroactive material. *IMA Journal of Applied Mathematics, 75*(4), 603–636.

Dorfmann, L., & Ogden, R. W. (2014). Instabilities of an electroelastic plate. *International Journal of Engineering Science, 77*, 79–101.

Dowaikh, M. A., & Ogden, R. W. (1991). On surface waves and deformations in a compressible elastic half-space. *Stability and Applied Analysis of Continuous Media, 1*(1), 27–45.

Gent, A. N. (1996). A new constitutive relation for rubber. *Rubber Chemistry and Technology, 69*(1), 59–61.

Greaney, P., Meere, M., & Zurlo, G. (2019). The out-of-plane behaviour of dielectric membranes: description of wrinkling and pull-in instabilities. *Journal of the Mechanics and Physics of Solids, 122*, 84–97.

Holzapfel, G. A. (2000). *Nonlinear Solid Mechanics: A Continuum Approach for Engineering*. Chichester: Wiley.

Horgan, C. O., & Saccomandi, G. (2004). Constitutive models for compressible nonlinearly elastic materials with limiting chain extensibility. *Journal of Elasticity, 77*, 123–138.

Huang, J. S., Li, T. F., Chiang Foo, C., Zhu, J., Clarke, D. R., & Suo, Z. G. (2012). Giant voltage actuated deformation of a dielectric elastomer under dead load. *Applied Physics Letters, 100*(4), Article 041911.

Keplinger, C., Kaltenbrunner, M., Arnold, N., & Bauer, S. (2010). Röntgen's electrode-free elastomer actuators without electromechanical pull-in instability. *Proceedings of the National Academy of Sciences, 107*(10), 4505–4510.

Koh, S. J. A., Li, T., Zhou, J., Zhao, X., Hong, W., Zhu, J., et al. (2011). Mechanisms of large actuation strain in dielectric elastomers. *Journal of Polymer Science Part B: Polymer Physics, 49*(7), 504–515.

Lee, S., Song, Y., Ko, Y., Ko, Y., Ko, J., Kwon, C. H., et al. (2020). A metal-like conductive elastomer with a hierarchical wrinkled structure. *Advanced Materials, 32*(7), Article 1906460.

Levinson, M., & Burgess, I. W. (1971). A comparison of some simple constitutive relations for slightly compressible rubber-like materials. *International Journal of Mechanical Sciences, 13*(6), 563–572.

Li, B., Zhou, J., & Chen, H. (2011). Electromechanical stability in charge-controlled dielectric elastomer actuation. *Applied Physics Letters, 99*(24), Article 244101.

Liu, L., Liu, Y., Leng, J., & Lau, K. (2011). Electromechanical stability of compressible dielectric elastomer actuators. *Smart Materials and Structures, 20*(11), Article 115015.

Liu, X. J., Li, B., Chen, H. L., Jia, S. H., & Zhou, J. X. (2016). Voltage-induced wrinkling behavior of dielectric elastomer. *Journal of Applied Polymer Science, 133*(14), 1–8.

Loeb, L. A., Amert, A. K., & Whites, K. W. (2014). Fabrication, measurement, and application of compressible artificial materials. *IEEE Transactions on Antennas & Propagation, 62*(12), 6140–6148.

Lu, T. Q., Cheng, M., & Wang, T. J. (2020). Mechanics of dielectric elastomer structures: A review. *Extreme Mechanics Letters, 38*, Article 100752.

Lu, T., Keplinger, C., Arnold, N., Bauer, S., & Suo, Z. (2014). Charge localization instability in a highly deformable dielectric elastomer. *Applied Physics Letters, 104*(2), Article 022905.

Mateiu, R. V., Yu, L., & Skov, A. L. (2017). Electrical breakdown phenomena of dielectric elastomers. In *Proc. In: SPIE, 10163. International Society for Optical Engineering*.

Mengüç, Y., Park, Y. L., Pei, H., Vogt, D., Aubin, P. M., Winchell, E., et al. (2014). Wearable soft sensing suit for human gait measurement. *The International Journal of Robotics Research, 33*(14), 1748–1764.

Mirvakili, S. M., & Hunter, I. W. (2018). Artificial muscles: Mechanisms, applications, and challenges. *Advanced Materials, 30*(6), Article 1704407.

Murphy, J. G., & Destrade, M. (2009). Surface waves and surface stability for a pre-stretched, unconstrained, non-linearly elastic half-space. *International Journal of Non-Linear Mechanics, 44*(5), 545–551.

Nah, C., Lee, G. B., Lim, J. Y., Kim, Y. H., SenGupta, R., & Gent, A. N. (2010). Problems in determining the elastic strain energy function for rubber. *International Journal of Non-Linear Mechanics, 45*(3), 232–235.

Nayfeh, A. H. (1995). *Wave propagation in layered anisotropic media: With application to composites*. Amsterdam: Elsevier.

Ogden, R. W. (1972). Large deformation isotropic elasticity: On the correlation of theory and experiment for compressible rubberlike solids. *Proceedings of the Royal Society of London. A. Mathematical and Physical Sciences, 328*(1575), 567–583.

Ogden, R. W., & Roxburgh, D. G. (1993). The effect of pre-stress on the vibration and stability of elastic plates. *International Journal of Engineering Science, 31*(12), 1611–1639.

Ogden, R. W., & Sotiropoulos, D. A. (1998). Reflection of plane waves from the boundary of a pre-stressed compressible elastic half-space. *IMA Journal of Applied Mathematics, 61*(1), 61–90.

Pelrine, R., Kornbluh, R., Pei, Q., & Joseph, J. (2000). High-speed electrically actuated elastomers with strain greater than 100%. *Science, 287*(5454), 836–839.

Plante, J. S., & Dubowsky, S. (2006). Large-scale failure modes of dielectric elastomer actuators. *International Journal of Solids and Structures, 43*(25), 7727–7751.

Rogovoy, A. (2001). Effect of elastomer slight compressibility. *European Journal of Mechanics-A/Solids, 20*(5), 757–775.

Rudykh, S., Bhattacharya, K., & deBotton, G. (2012). Snap-through actuation of thick-wall electroactive balloons. *International Journal of Non-Linear Mechanics, 47*(2), 206–209.

Rudykh, S., & Debotton, G. (2011). Stability of anisotropic electroactive polymers with application to layered media. *Zeitschrift für angewandte Mathematik und Physik, 62*(6), 1131–1142.

Rus, D., & Tolley, M. T. (2015). Design, fabrication and control of soft robots. *Nature, 521*(7553), 467–475.

Shuvalov, A. L. (2000). On the theory of wave propagation in anisotropic plates. *Proceedings of the Royal Society of London. Series A: Mathematical, Physical and Engineering Sciences, 456*(2001), 2197–2222.

Stark, K. H., & Garton, C. G. (1955). Electric strength of irradiated polythene. *Nature, 176*(4495), 1225–1226.

Su, Y. P., Chen, W. Q., & Destrade, M. (2019). Tuning the pull-in instability of soft dielectric elastomers through loading protocols. *International Journal of Non-Linear Mechanics, 113*, 62–66.

Su, Y. (2020). Voltage-controlled instability transitions and competitions in a finitely deformed dielectric elastomer tube. *International Journal of Engineering Science, 157*, Article 103380.

Su, Y., Conroy Broderick, H., Chen, W., & Destrade, M. (2018b). Wrinkles in soft dielectric plates. *Journal of the Mechanics and Physics of Solids, 119*, 298–318.

Su, Y., Wu, B., Chen, W., & Lü, C. (2018a). Optimizing parameters to achieve giant deformation of an incompressible dielectric elastomeric plate. *Extreme Mechanics Letters, 22*, 60–68.

Toupin, R. A. (1956). The Elastic Dielectric. *Journal of Rational Mechanics and Analysis, 5*(6), 849–915.

Wan, Y., Qiu, Z., Huang, J., Yang, J., Wang, Q., Lu, P., et al. (2018). Natural plant materials as dielectric layer for highly sensitive flexible electronic skin. *Small, 14*(35), Article 1801657.

Xia, G., Huang, Y., Su, Y., & Chen, W. (2020). Exact axisymmetric adhesive contact analysis for a pre-deformed soft electroactive half-space. *International Journal of Solids and Structures, 207*, 206–229.

Yang, J., Tang, D., Ao, J., Ghosh, T., Neumann, T. V., Zhang, D., et al. (2020). Ultrasoft liquid metal elastomer foams with positive and negative piezopermittivity for tactile sensing. *Advanced Functional Materials, 30*(36), Article 2002611.

Yang, S., Zhao, X., & Sharma, P. (2017). Revisiting the instability and bifurcation behavior of soft dielectrics. *Journal of Applied Mechanics-Transaction of the ASME, 84*(3), Article 031008.

Zhang, J., Zhao, J., Wang, S., Chen, H., & Li, D. (2017). Large stable deformation of dielectric elastomers driven on mode of steady electric field. *Smart Materials and Structures, 26*(5), 05LT01.

Zhao, X., & Suo, Z. (2007). Method to analyze electromechanical stability of dielectric elastomers. *Applied Physics Letters, 91*(6), Article 061921.

Zhou, J. X., Hong, W., Zhao, X. H., Zhang, Z. Q., & Suo, Z. G. (2008). Propagation of instability in dielectric elastomers. *International Journal of Solids and Structures, 45*(13), 3739–3750.

Zhou, J., Jiang, L., & Cai, S. (2020). Predicting the electrical breakdown strength of elastomers. *Extreme Mechanics Letters, 34*, Article 100583.

Zhu, F., Zhang, C., Qian, J., & Chen, W. (2016). Mechanics of dielectric elastomers: Materials, structures, and devices. *Journal of Zhejiang University SCIENCE A, 17*(1), 1–21.

Zurlo, G., Destrade, M., & Lu, T. (2018). Fine tuning the electro-mechanical response of dielectric elastomers. *Applied Physics Letters, 113*, Article 162902.